scientific reports

Check for updates

OPEN

Design, synthesis, and evaluation of novel substituted imidazo[1,2-*c*]quinazoline derivatives as potential *α*-glucosidase inhibitors with bioactivity and molecular docking insights

Fariba Peytam[1], Faezeh Sadat Hosseini[1], Reza Fathimolladehi[2], Mohammad Javad Dehghan Nayeri[3], Mahdis Sadeghi Moghadam[1], Bahareh Bayati[1], Maryam Norouzbahari[4], Roham Foroumadi[5], Fahimeh Bonyasi[2], Ruzbehan Divsalar[6], Somayeh Mojtabavi[7], Mohammad Ali Faramarzi[7], Maliheh Barazandeh Tehrani[2], Loghman Firoozpour[1,2]✉ & Alireza Foroumadi[1,6]✉

α-Glucosidase inhibitors are important in the treatment of type 2 diabetes by regulating blood glucose levels and reducing carbohydrate absorption. The present study focuses on identifying new inhibitors bearing imidazo[1,2-*c*]quinazoline backbone through multi-step synthesis. The inhibitory potencies of the novel derivatives were tested against *Saccharomyces cerevisiae* α-glucosidase, revealing IC_{50} values ranging from 50.0 ± 0.12 μM to 268.25 ± 0.09 μM. Among them, 2-(4-(((2,3-diphenylimidazo[1,2-*c*]quinazolin-5-yl)thio)methyl)-1*H*-1,2,3-triazol-1-yl)-*N*-(2-methoxyphenyl)acetamide (19e) and 2-(4-((benzo[4,5]imidazo[1,2-*c*]quinazolin-6-ylthio)methyl)-1*H*-1,2,3-triazol-1-yl)-*N*-(2-methoxyphenyl)acetamide (27e) emerged as the most potent inhibitors and were further investigated in various assessments. Finally, molecular docking studies were performed to reveal the crucial binding interactions and to confirm the results obtained from structure-activity relationship (SAR) analysis.

Keywords Diabetes, *α*-Glucosidase, Imidazo[1,2-*c*]quinazoline, Imidazoquinazoline

Diabetes mellitus (DM) is a complex and chronic metabolic condition which requires continuous medical care alongside a range of multifactorial risk-reduction strategies, particularly those related to glucose regulation[1]. Moreover, it is associated with various diseases, including cardiovascular disorders, kidney failure, neuropathy, lipid metabolism disorders, and other health-related complications[2]. The global prevalence of diabetes has remarkably increased from 108 million in 1980 to 422 million in 2014, which is 8.5% of adults with different age. From 2000 to 2019, there was a 3% increase in diabetes-related mortality rates, and it had become the direct cause of 1.5 million deaths in 2019. Moreover, the raised blood glucose resulted from diabetes has been proved to indirectly contribute to mortality; for instance, almost 20% of cardiovascular-related deaths can be attributed to diabetes[3].

Diabetes is classified into various groups, including type 1, type 2, maturity-onset diabetes of the young (MODY), gestational diabetes, neonatal diabetes, and steroid-induced diabetes. Among these types, diabetes

[1]Drug Design and Development Research Center, The Institute of Pharmaceutical Sciences (TIPS), Tehran University of Medical Sciences, Tehran, Iran. [2]Department of Medicinal Chemistry, Faculty of Pharmacy, Tehran University of Medical Sciences, Tehran, Iran. [3]Department of Biology, Faculty of Natural Science, University of Tabriz, Tabriz 5166616471, Iran. [4]Faculty of Pharmacy, Final International University, Catalkoy, Kyrenia via Mersin 10 Turkey, Turkish Republic of Northern Cyprus. [5]Department of Pharmacology, School of Medicine, Tehran University of Medical Sciences, Tehran, Iran. [6]Neuroscience Research Center, Institute of Neuropharmacology, Kerman University of Medical Sciences, Kerman, Iran. [7]Department of Pharmaceutical Biotechnology, Faculty of Pharmacy, Tehran University of Medical Sciences, Tehran, Iran. ✉email: firoozpour@gmail.com; aforoumadi@yahoo.com

mellitus type 2 (T2DM) is the most prevalent, accounting for over 95% of cases. In the past three decades, the global prevalence of T2DM has risen significantly. Historically, T2DM was predominantly observed in adults; however, there has been an increasing occurrence of this type of diabetes in children. Therefore, there is a globally acknowledged goal to decrease the rise in the rates of diabetes and obesity by 2025[3].

A key strategy in managing hyperglycemia caused by T2DM involves disrupting the breakdown of dietary carbohydrates. α-Glucosidase, an enzyme located in the brush border of the intestine, plays a substantial role in breaking down complex sugars into monosaccharide units, which are subsequently released into the bloodstream. Therefore, an approved treatment for T2DM involves the inhibition of α-glucosidase to slow down glucose absorption, thereby reducing postprandial glucose levels. Additionally, according to the guidelines of International Diabetes Federation, α-glucosidase inhibitors, alongside insulin, metformin, and sulfonylureas, are considered optional treatments for managing uncontrolled hyperglycemia in patients with T2DM[4].

All α-glucosidase inhibitors function in a dose-dependent and comparable mechanisms of action, although they exhibit some differences. These agents compete to bind to the active site of enzymes, resulting in interference with the cleavage of oligosaccharides and the subsequent formation of monosaccharides. Currently, acarbose, voglibose, miglitol, and emiglitate are examples of commercial drugs used to manage postprandial hyperglycemia. Among these drugs, acarbose has been the subject of the most extensive study. Despite its efficacy to inhibit α-glucosidase performance, its use is associated with various side effects, including diarrhea, vomiting, flatulence, severe stomach pain, and allergic reactions[5]. Therefore, discovery and development of novel α-glucosidase inhibitors that possess high potency and minimal side effects is highly demanding. In recent decades, numerous aza-heterocyclic compounds[6–14], particularly those bearing substituted quinazolines[15–30]and substituted imidazoles[31–40], have been identified as exhibiting significant α-glucosidase inhibitory activities.

Hybridization strategy is a pivotal synthetic method in recent drug discovery and development process, wherein two or more pharmacophores are combined to prepare further bioactive small molecules. This approach aims not only to overcome the limitations of individual compounds but also to increase their potency and selectivity[41]. On the other hand, 1,2,3-triazoles have emerged as a noticeable pharmacophore in chemical biology and drug discovery in recent years. Their unique structural abilities to form pivotal protein-ligand interactions, including hydrogen bonding and pi-based interactions, alongside their facile and efficient synthesis through click reaction have made 1,2,3-triazoles a key building block for the preparation of small molecules focusing various therapeutic targets[42]. Regarding the significance of hybridization strategy alongside the remarkable features of 1,2,3-triazoles, this core has been widely used in numerous bioactive compounds. For example, several substituted quinazolines and imidazoles have been incorporated with 1,2,3-triazoles, leading to the identification of potential α-glucosidase inhibitors (Fig. 1)[43–48].

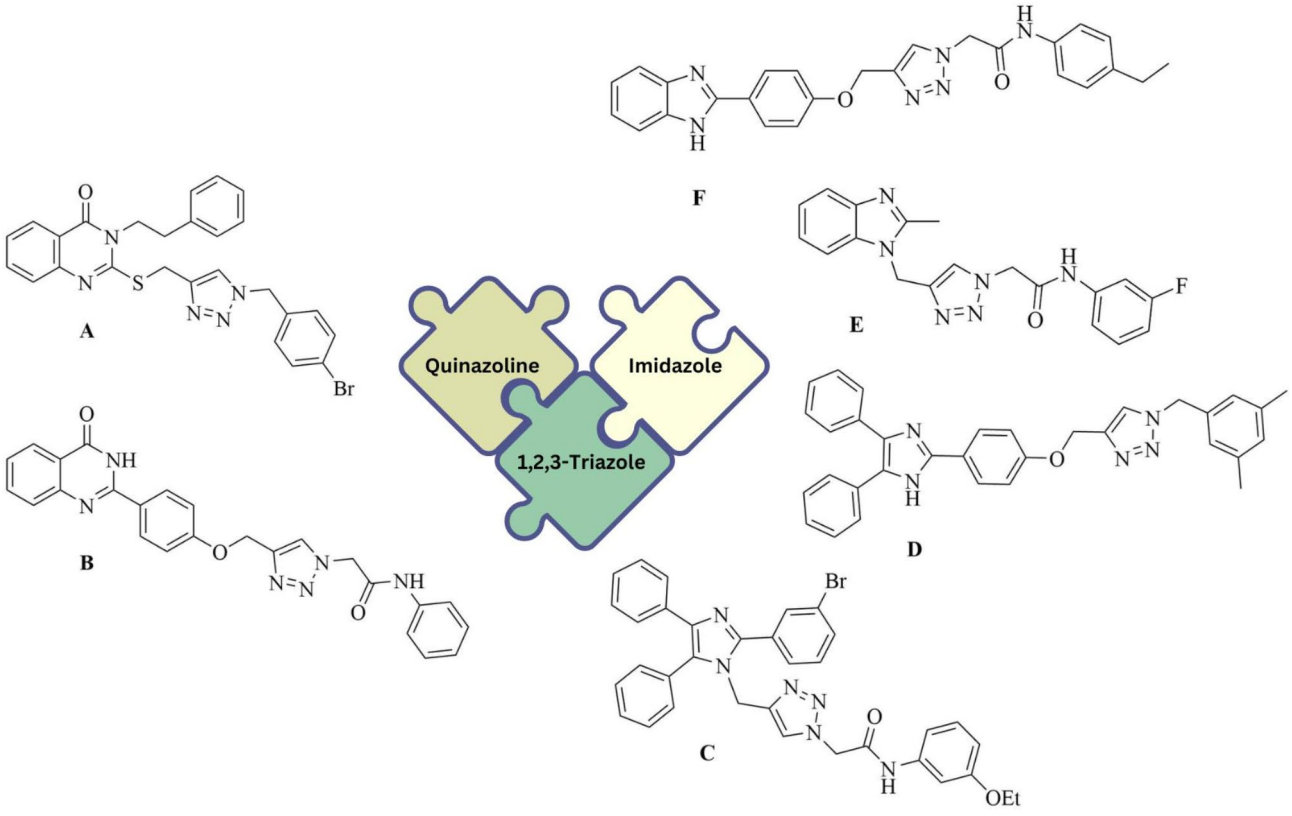

Fig. 1. α-Glucosidase inhibitors bearing several substituted quinazolines and imidazoles incorporated with 1,2,3-triazoles.

As a part of our continuing investigation into the α-glucosidase inhibitors[49–53], we previously combined imidazole and quinazoline into one scaffold, resulting in the synthesis of substituted imidazo[1,2-*c*]quinazolines and introduction of this backbone as promising inhibitors[54]. As previously described, the substituents on C-5 position of this backbone played a key role on the α-glucosidase inhibition. Consequently, we followed our investigation by incorporating the substituted 1,2,3-triazoles at this position to identify further potential inhibitors (Fig. 2).

In the present study, we employed an efficient synthetic approach to prepare several series of imidazoquinazolines and evaluate their *in-vitro* activities against α-glucosidase. To provide a comprehensive structure-activity relationship analysis, our compounds were divided into two general categories: poly-substituted imidazo[1,2-*c*]quinazolines and benzo[4,5]imidazo[1,2-*c*]quinazolines. Each series was further subdivided into three groups: (1) compounds **15** and **24**, bearing an amide functionality tail; (2) compounds **18** and **26**, bearing a 1-aryl-1*H*-1,2,3-triazole tail; (3) compounds **19** and **27**, bearing a (1*H*-1,2,3-triazol-1-yl)-*N*-arylacetamide tail. Based on the enzymatic inhibitory potencies, compounds **19e** and **27e** were selected for further evaluations, including kinetic study, circular dichroism measurement, fluorescence quenching measurements, and thermodynamic analysis of their binding to α-glucosidase. Finally, comprehensive molecular docking studies were performed to elucidate the mode of interactions between our compounds and enzyme binding site, as well as to highlight the role of different components of the scaffold.

Results and discussion

Chemistry

To synthesize the targeted multi-substituted imidazo[1,2-*c*]quinazolines **15**, **18**, **19**, **24**, **26**, and **27**, several efficient synthetic routes were conducted under the mild conditions (Fig. 3). Initially, a mixture of substituted anilines **1a-h** and chloroacetyl chloride **2** in the presence of triethylamine (Et_3N) were stirred at ambient temperature in acetone within overnight to obtain substituted 2-chloro-*N*-arylacetamide **3a-h**, followed by the bimolecular nucleophilic substitution (S_N2) with sodium azide (NaN_3) **4** to afford substituted 2-azido-*N*-arylacetamide **5a-h**. Additionally, substituted benzylazides **7a-c** were synthesized through S_N2 reaction between corresponding substituted benzylbromides **6a-c** and NaN_3, which was performed in the presence of Et_3N in Dimethylformamide (DMF) within 2h.

The synthesis of first series of substituted imidazo[1,2-*c*]quinazolines, as illustrated in scheme 1-part B, was initiated with a cyclization reaction between 2-nitrobenzaldehyde **8**, ammonium acetate **9**, and benzil **10** under reflux in glacial acetic acid (HOAc) to obtain the 2-(2-nitrophenyl)-4,5-diphenyl-1*H*-imidazole **11**. To prepare the similar compound from second series (2-(2-nitro,phenyl)-1*H*-benzo[d]imidazole **21**), a cyclization reaction between 2-nitrobenzaldehyde **8** and benzene-1,2-diamine **20** was performed in the presence of catalytic amount of HOAc in ethanol (EtOH) under reflux. The conditions of subsequent steps for both parts B and C were common.

The nitro functionality in compounds **11** and **21** was reduced to amine moiety using stannous chloride dihydrate ($SnCl_2.2H_2O$) and hydrochloric acid in methanol at ambient temperature within 6h to afford compounds **12** and **22**, which subsequently went through the cyclization using carbon disulfide **13** and potassium hydroxide (KOH) in EtOH under reflux for approximately 3h to obtain the corresponding imidazo[1,2-*c*]quinazoline-5-thiol (compounds **14** and **23**). Afterwards, they underwent two types of S_N2 reactions in the presence of potassium carbonate (K_2CO_3) in DMF at 80 °C for 12h. The first reaction involved derivatives of 2-chloro-N-arylacetamide (compound 3), leading to products **15a-c** and **24a-c**, which contained only the amide moiety. The second reaction utilized propargyl bromide (compound **16**) to produce compounds **17** and **25** having acetylene moiety. These compounds then went through click reaction with previously prepared compounds **5a-h** and **7a-c** in the presence of $CuSO_4.5H_2O$ and sodium ascorbate in DMF at room temperature within 12h. Consequently, the desired poly-substituted imidazo[1,2-*c*]quinazolines bearing 1,2,3-triazole ring (**18a-c**, **19a-h**, **26a-c**, and **27a-h**) were prepared.

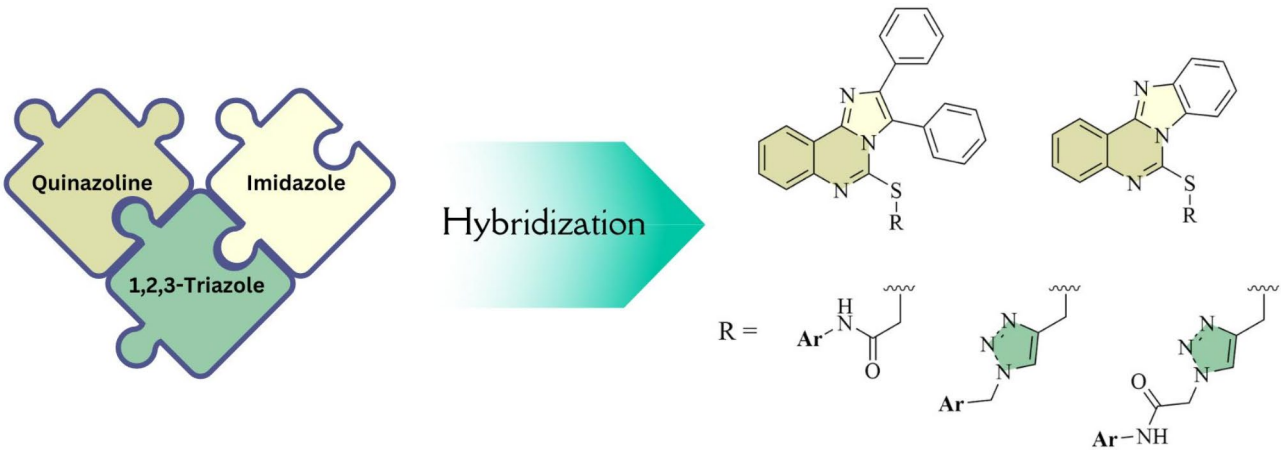

Fig. 2. Design strategy of novel imidazo[1,2-*c*]quinazoline derivatives as potential α-glucosidase inhibitors.

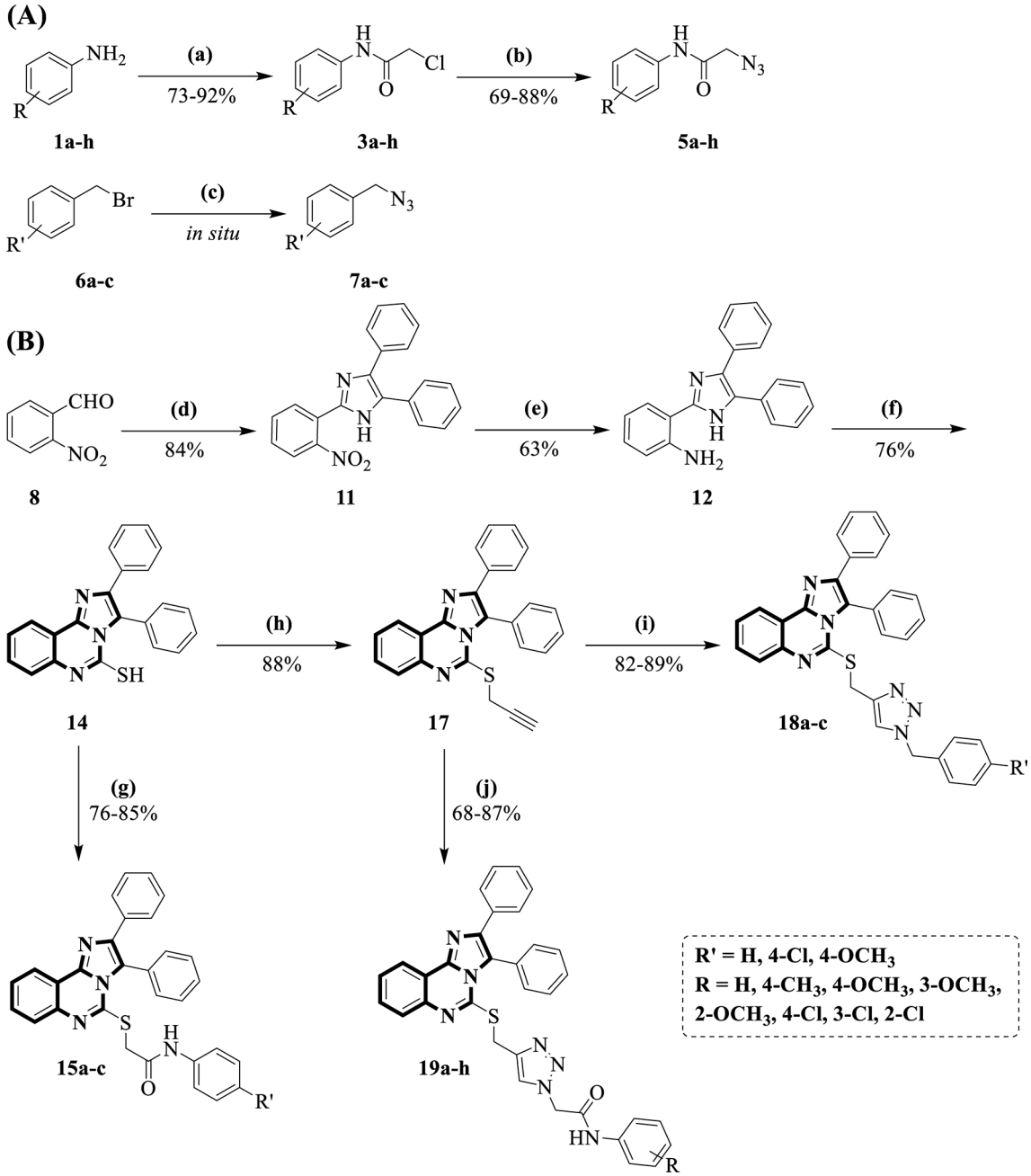

Fig. 3. Reaction conditions and reagents: (**a**) chloroacetyl chloride **2**, Et_3N, acetone, r.t., overnight; (**b**) NaN_3**4**, DMF, r.t., overnight; (**c**) NaN_3**4**, DMF, r.t., 2h; (**d**) ammonium acetate **9**, benzil **10**, HOAc, reflux, 10h; (**e**) $SnCl_2.2H_2O$, HCl, MeOH, r.t., 6h; (**f**) CS_2**13**, KOH, EtOH, reflux, 3h; (**g**) 2-chloro-*N*-arylacetamide **3**, K_2CO_3, DMF, 80 °C, 12h; (**h**) propargyl bromide **16**, K_2CO_3, DMF, 80 °C, 12h; (**i**) 2-azido-*N*-arylacetamide **5**, $CuSO_4.5H_2O$, sodium ascorbate, DMF, r.t., overnight; (**j**) substituted benzyl azides **7**, $CuSO_4.5H_2O$, sodium ascorbate, DMF, r.t., overnight; (**k**) benzene-1,2-diamine **20**, HOAc (20 mol%), EtOH, reflux, 10h.

The structures of the isolated compounds **15a-c**, **18a-c**, **19a-h**, **24a-c**, **26a-c**, and **27a-h** were completely deduced on the basis of their IR, ^1H and ^{13}C NMR spectroscopy, as well as high-resolution mass spectrometry (HRMS) and elemental analysis. Partial assignments of these resonances are given in the Experimental Part.

In vitro α-glucosidase inhibitory activity

Several series of substituted imidazo[1,2-*c*]quinazolines **15**, **18**, **19**, **24**, **26**, and **27** were synthesized to assess their *in vitro* inhibitory activities against *Saccharomyces cerevisiae* α-glucosidase and compare their results with acarbose as a standard drug. Various derivatives were prepared to investigate the presence of one or two phenyl rings on the imidazoquinazoline backbone, the presence of amide functionality, the presence of triazole ring, and the role of substituents on the terminal phenyl rings. The results were summarized in Tables 1 and 2.

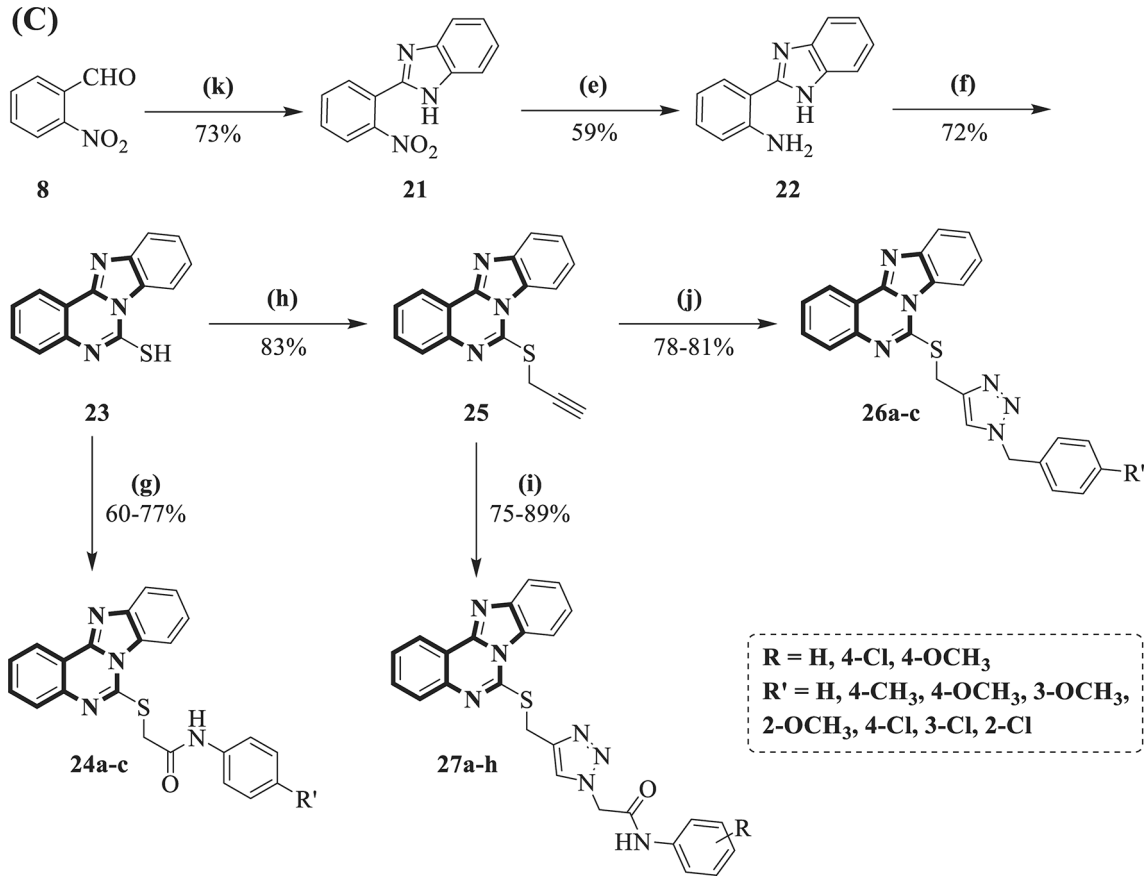

Figure 3. (continued)

As presented, all compounds demonstrated good to excellent inhibitory activities with IC_{50} values ranging from 50.0 ± 0.12 µM to 268.25 ± 0.09 µM, showing better potencies in comparison to the acarbose with IC_{50} value of 750.0 ± 1.5 µM. To describe the correlations between structures and observed activities, compounds were divided into three categories according to the substituents linked to the sulfur atom. Furthermore, each table's compounds were subdivided into two groups, considering the substituents on the imidazole moiety of imidazoquinazoline backbone: derivatives bearing two phenyl rings were depicted on the right part, and derivatives bearing one fused phenyl ring were depicted on the left part. In both tables, compounds belonging to the first group exhibited superior inhibition potencies compared to their counterparts in the second group.

As illustrated in Table 1, compounds **19** and **27** featured both amide functionality and 1,2,3-triazole ring, and our goal was to examine the impact of substituents on the terminal phenyl ring. In the left series, compound **19a** bearing unsubstituted phenyl ring displayed significant inhibitory activity (IC_{50} = 118.25 ± 0.04 µM). Introducing a methyl group (CH_3) at C-4 position of this phenyl caused a decrease in potency; whereas incorporating a methoxy group (OCH_3) at same position yielded compound **19c** with enhanced activity (IC_{50} = 89.30 ± 0.34 µM). Further exploration involved the introduction of this group at other ring positions: C-3 position in compound **19d** and C-2 position in compound **19e**, both of which led to improved inhibitory activity. Notably, compound **19e**, bearing 2- OCH_3, exhibited the greatest inhibition potency (IC_{50} = 50.0 ± 0.12 µM), emerging as the most potent derivative in the present study and being 15 times more potent than acarbose, the standard drug for *α*-glucosidase inhibition. Subsequently, a chlorine atom was introduced at different positions on the terminal phenyl ring, resulting in compounds **19f**, **19g**, and **19h**, which showed weaker inhibitory activities compared to their analogues bearing the OCH_3 group.

Within the right series, compounds **27**, bearing benzo[4,5]imidazo[1,2-*c*]quinazoline backbone, showed great inhibitory activities. The presence of unsubstituted phenyl ring led to compound **27a** with good potency (IC_{50} = 122.25 ± 0.13 µM). Incorporating the C-4 position of terminal phenyl ring with any substituents (methyl in compound **27b**, methoxy in compound **27c**, and chlorine in compound **27f**) caused the detrimental effects on the inhibition activities. Shifting the methoxy group to the C-3 position of this phenyl ring led to compound **27d** with enhanced potency, while the presence of chlorine at this position (compound **27g**) further decreased the potency. Regarding the C-2 position, introducing the methoxy group resulted in compound **27e** exhibiting the best inhibitory activity in this series (IC_{50} = 60.03 ± 0.82 µM). Notably, this compound was the second most potent compound in present study. However, substituting the terminal phenyl ring with 2-Cl in compound **27h**, with IC_{50} value of 123.39 ± 0.58 µM, did not yield to any improvement in comparison with compound **27a** (IC_{50} = 122.25 ± 0.13 µM).

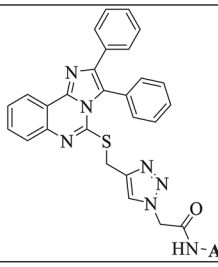

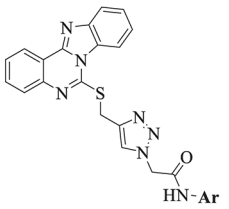

Label	Ar	IC_{50} (μM)	Label	Ar	IC_{50} (μM)
19a		118.25 ± 0.04	**27a**		122.25 ± 0.13
19b	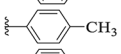	137.90 ± 0.20	**27b**	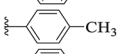	192.25 ± 0.48
19c	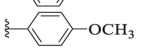	89.30 ± 0.34	**27c**	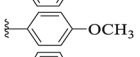	148.63 ± 0.06
19d	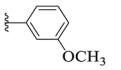	72.78 ± 0.16	**27d**	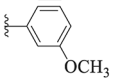	80.37 ± 0.53
19e		50.0 ± 0.12	**27e**		60.03 ± 0.82
19f	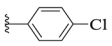	126.28 ± 0.09	**27f**	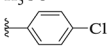	245.32 ± 0.38
19g	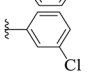	96.89 ± 0.23	**27g**	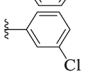	194.76 ± 0.63
19h		77.23 ± 0.80	**27h**		123.39 ± 0.58
Acarbose		750.0 ± 2.1	**Acarbose**		750.0 ± 2.1

[a] Values are the mean ± SD. All experiments were performed at least three times.

Table 1. Substrate scope and *in vitro* α-glucosidase inhibitory activity of compounds **19a-h** and **27a-h**.

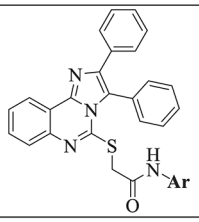

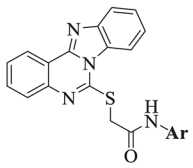

Label	Ar	IC_{50} (μM)	Label	Ar	IC_{50} (μM)
15a		196.85 ± 0.08	**24a**		268.25 ± 0.09
15b	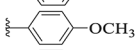	124.73 ± 0.49	**24b**	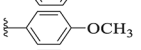	198.49 ± 0.38
15c	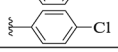	175.05 ± 1.02	**24c**	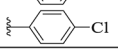	186.32 ± 0.56

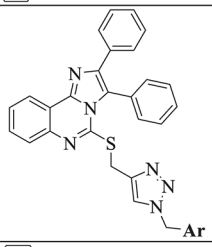

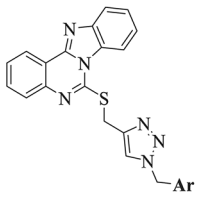

18a		174.43 ± 1.16	**26a**		224.35 ± 0.13
18b	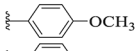	148.64 ± 0.38	**26b**	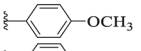	173.28 ± 1.02
18c	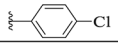	96.05 ± 0.72	**26c**	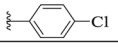	124.32 ± 0.05
Acarbose		750.0 ± 1.5	**Acarbose**		750.0 ± 1.5

[a] Values are the mean ± SD. All experiments were performed at least three times.

Table 2. Substrate scope and *in vitro* α-glucosidase inhibitory activity of compounds **15** and **24**.

After investigating the impact of substituents on the terminal phenyl ring, the substantial contributions of amide functional group and 1,2,3-triazole ring were examined, and compounds were synthesized bearing only one of these moieties. For example, compounds **15** and **24** were obtained by eliminating the triazole, while compounds **18** and **26** were synthesized by removing the amide functionality. Notably, all these compounds, with the exception of compound **18c**, exhibited weaker inhibition potencies than their analogues listed in the Table 1. Within the subgroup of compounds bearing the amide group (**15** and **24**), compound **15b** exhibited the highest inhibitory potency. Conversely, among the compounds containing the triazole moiety (**18** and **26**), compound **18c** demonstrated the most potent inhibition.

In summary, our SAR analysis revealed that incorporating two phenyl rings connected to the imidazole moiety of imidazo[1,2-*c*]quinazoline significantly led to improved inhibitory activity. Moreover, the presence of both amide functionality and 1,2,3-triazole proved pivotal role for enhancing inhibitory efficacy. Regarding the role of substituents on the terminal phenyl ring, the introduction of methoxy group at C-2 position modified the inhibition potency. Compounds **19e** and **27e** emerged as the most potent inhibitors against *α*-glucosidase, showing IC_{50} values of 50.0 ± 0.12 µM and 60.03 ± 0.82 µM, respectively. These compounds exhibited substantially greater potency compared to acarbose, the reference drug for *α*-glucosidase inhibition; therefore, they can be appropriate candidates for further evaluations in present study.

Enzyme kinetic study

To elucidate the inhibition mode of imidazoquinazolines **19** and **27**, an enzyme kinetic study was conducted on the most active compounds, **19e** and **27e** (Fig. 4). This investigation involved varying concentrations of p-nitrophenyl α-D-glucopyranoside (1–16 mM) as the substrate, both in the absence and presence of compound **19e** (0, 12.5, 25, and 50 µM) and compound **27e** (0, 15, 30, and 60 µM). The Lineweaver–Burk plot was outlined in Fig. 3. As the concentrations of these inhibitors increased, the K_m value increased, whereas V_{max} remained constant. These findings revealed that imidazoquinazolines **19e** and **27e** bind to the active site of *α*-glucosidase, indicating their competitive inhibition and competing with acarbose to occupy this region. Furthermore, plotting

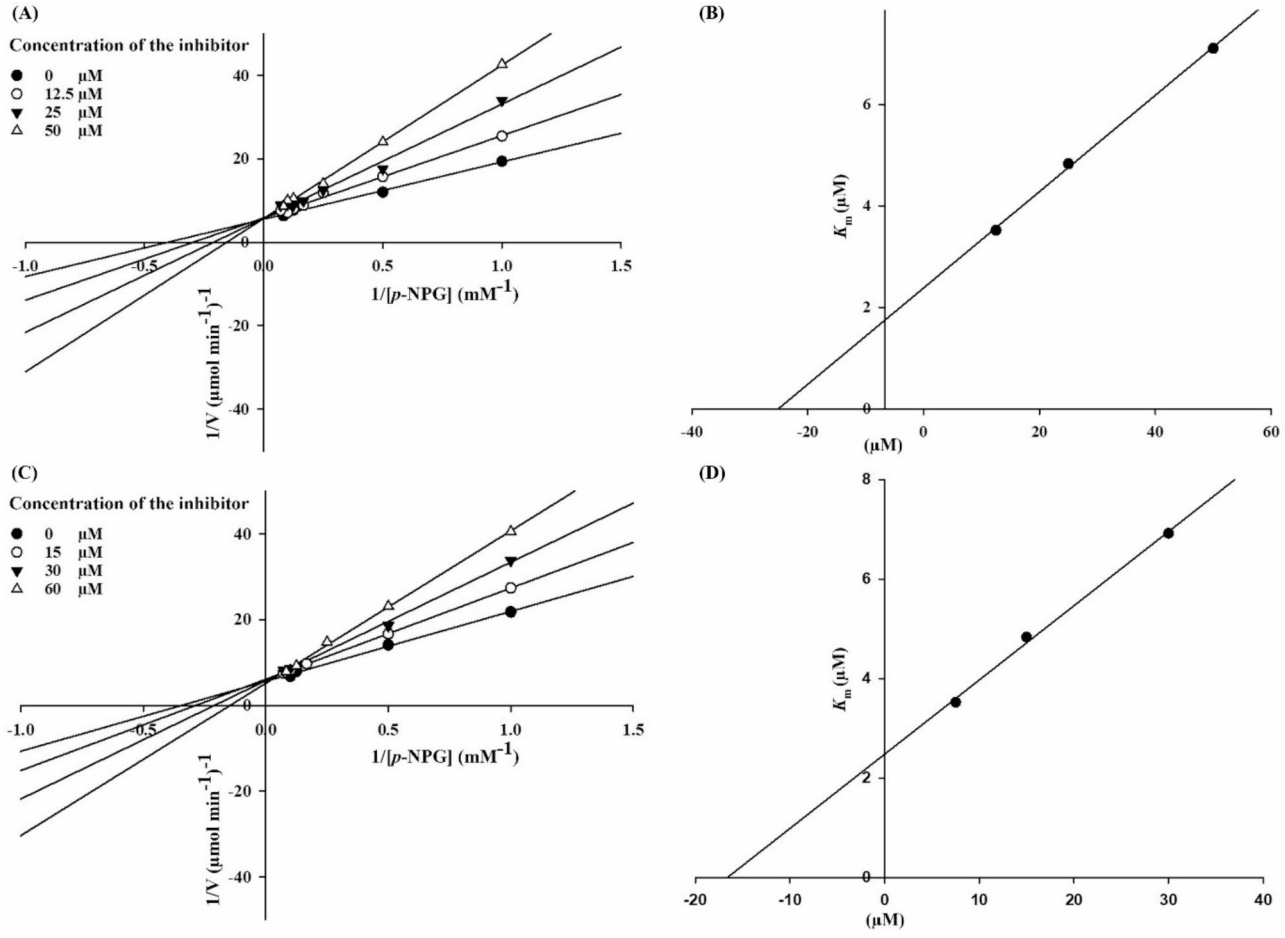

Fig. 4. Kinetics of *α*-glucosidase inhibition by imidazoquinazolines **19e** and **27e**: (**A**) The Lineweaver–Burk plot in the absence and presence of different concentrations of compound **19e**; (**B**) The secondary plot between K_m and various concentrations of compound **19e**; (**C**) The Lineweaver–Burk plot in the absence and presence of different concentrations of compound **27e**; (**D**) The secondary plot between K_m and various concentrations of compound **27e**.

K_m against various concentrations imidazoquinazolines **19e** and **27e** resulted into an estimated inhibition constant, yielding a K_i value of 25.0 μM for compound **19e** and a K_i value of 12.0 μM for compound **27e**.

Circular dichroism spectroscopy assessment

To indicate the chiral environment next to the enzyme amino acid residues of, an instrumental technique, named circular dichroism spectroscopy (CD), is employed by measuring the difference in absorption between right and left polarized light. There are various types of CD, one of which is measured in the far ultraviolet (UV) region ranging from 190 nm to 240 nm. This type offers crucial information about the arrangement of protein bonds and secondary structure of the proteins in dilute solutions. Considering characteristic CD signatures, proteins exhibit several principal conformations, including *α*-helix, extended *β* structure (or *β*-sheet), *β*-turn, and random coil (which are unordered structures). The type of conformation in the CD spectra is determined based on the specific wavelengths. For example, *α*-helix is characterized by negative CD bands observed at 222 nm and 208 nm, along with a positive CD band around 190 nm. The *β*-turn is identified by a negative CD band between 180 nm and 190 nm. Random coil is recognized by a characteristic negative CD band around region of 200 nm[55,56].

In present study, the CD spectra ranging from 180 nm to 250 nm were measured and analyzed using CDNN software in the presence of native *α*-glucosidase (Fig. 5a), enzyme exposed to imidazo[1,2-*c*]quinazole **19e** (Fig. 5b), and enzyme exposed to benzo[4,5]imidazo[1,2-*c*]quinazoline **27e** (Fig. 5c). Moreover, the percent of observed conformations are listed in Table 3. Comparing with native *α*-glucosidase, the percent of *β*-turn conformation increased for both compounds **19e** and **27e**; whereas the percent of *α*-helix conformation did not have any specific change, and the percent of random coil conformations decreased significantly. These results revealed that imidazoquinazolines **19e** and **27e** could determine the conformations of *α*-glucosidase and fix chiral side chains in the orientation of *β*-turn. Therefore, compounds **19e** and **27e** could inhibit *α*-glucosidase by altering the secondary structure of enzyme.

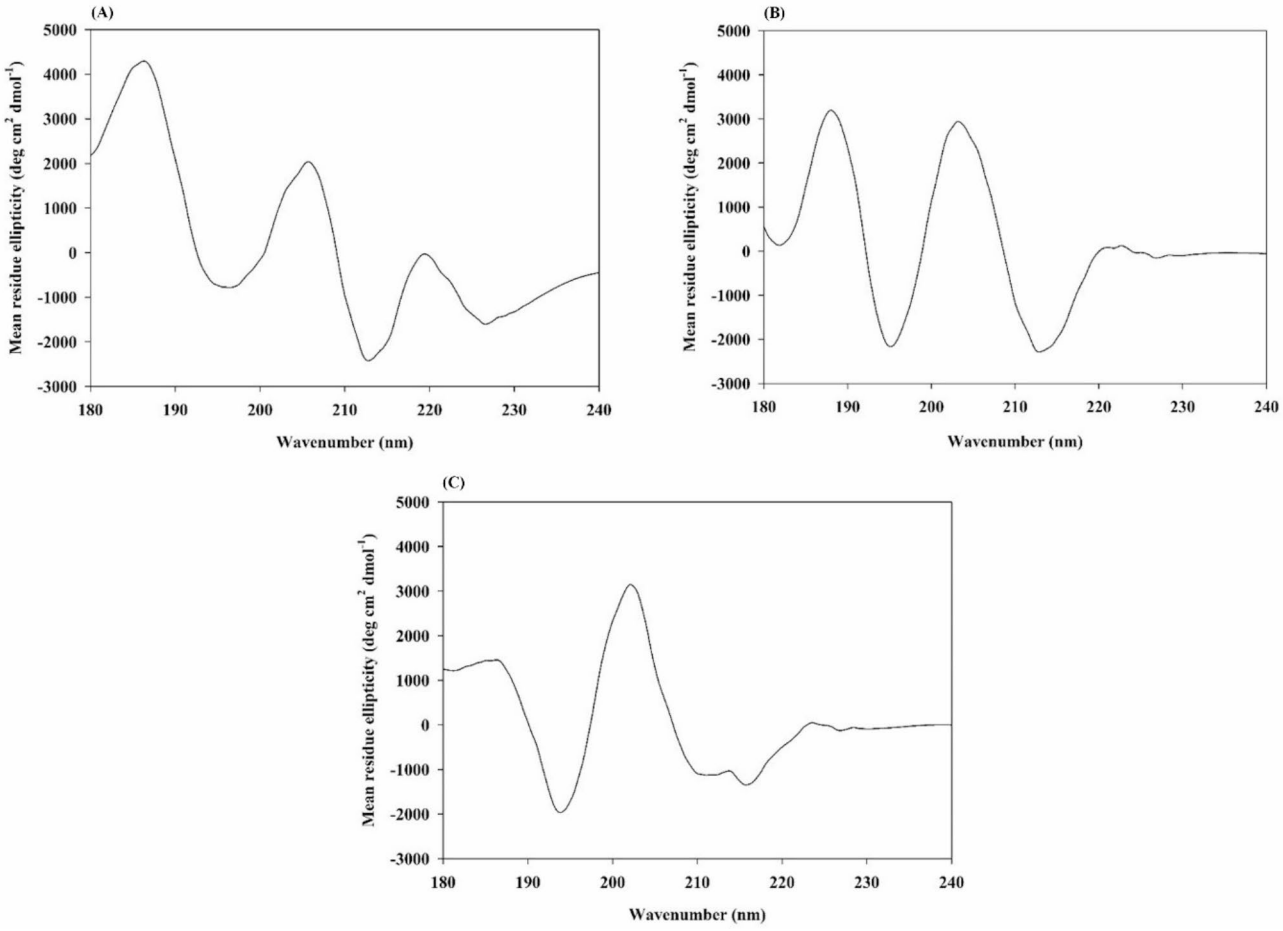

Fig. 5. Circular dichroism (CD) spectra of the *α*-glucosidase: (**A**) in the absence of inhibitor (control); (**B**) in the presence of imidazo[1,2-*c*]quinazole **19e** at the concentration of 50 μM; (**C**) in the presence of benzo[4,5] imidazo[1,2-*c*]quinazoline **27e** at the concentration of 60 μM.

Inhibitor	α-Helix (%)	β-Turn (%)	Random Coil (%)
Control[a]	28.8	28.8	42.4
imidazoquinazoline **19e**[b]	28.9	46.9	24.2
imidazoquinazoline **27e**[c]	32.1	54.9	13

Table 3. The secondary structure content of α-glucosidase. [a]Control is native enzyme in the absence of an inhibitor. [b]The concentration of imidazoquinazoline **19e** was 50 μM. [c]The concentration of imidazoquinazoline **27e** was 60 μM.

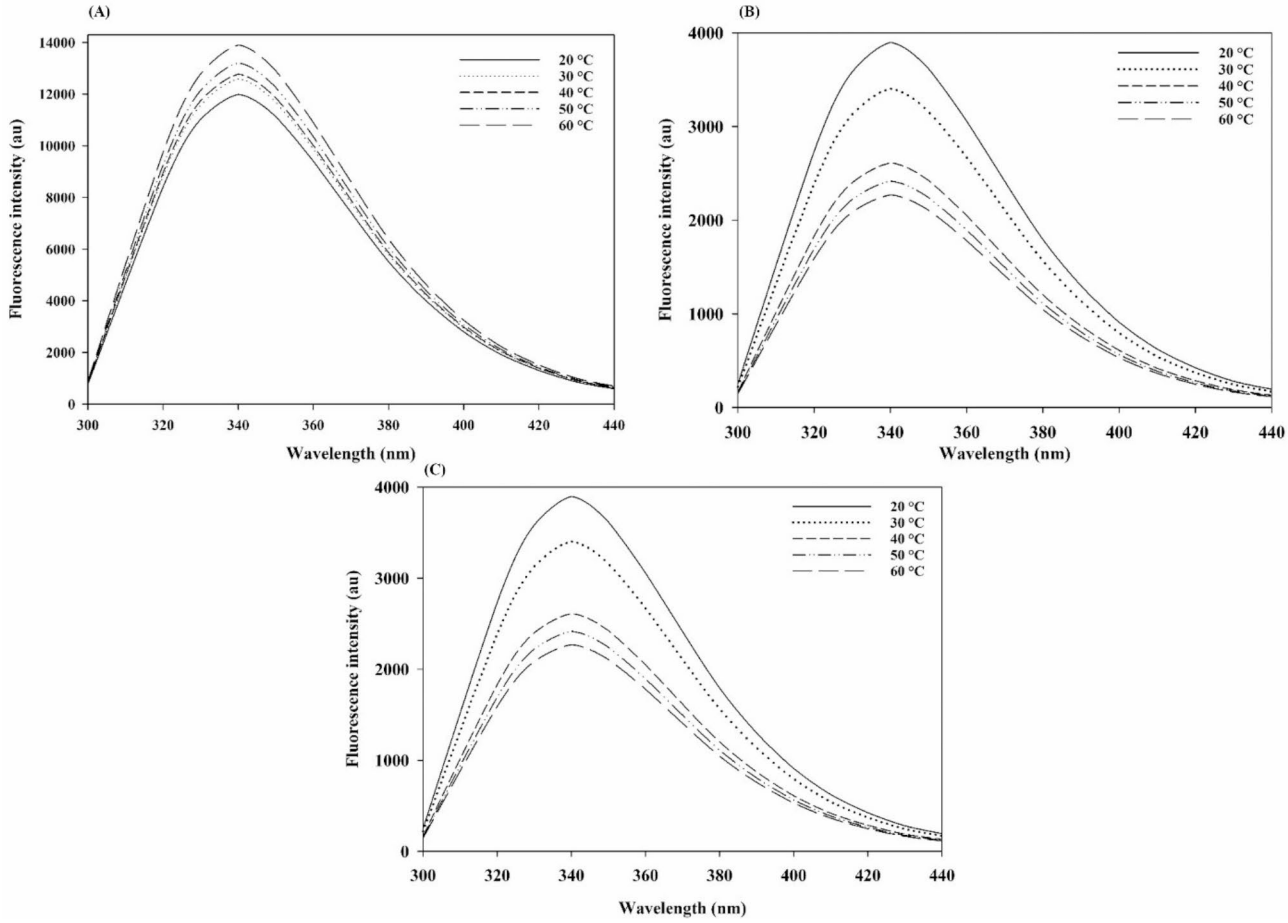

Fig. 6. Fluorescence spectra of α-glucosidase at 20–60 °C: (**A**) in the absence of any inhibitor (control); (**B**) enzyme exposed to imidazo[1,2-*c*]quinazole **19e** at the concentration of 50 μM; (**C**) enzyme exposed to benzo[4,5]imidazo[1,2-*c*]quinazoline **27e** at the concentration of 60 μM.

Fluorescence spectroscopy measurements

Fluorescence spectroscopy measurements are a traditional technique mainly used to explore the potential inhibitors and enzymes under the physiological conditions. As a consequence of binding the inhibitors to the active site of enzymes, the fluorescence characteristics and tertiary structure of the protein change, leading to fluorescence quenching which refers to any process which reduces the fluorescence intensity of an enzyme. This quenching caused by various reasons, including the collisional encounter between the fluorophore and the quencher (called dynamic quenching), formation of ground-state complex between fluorophore and quencher (called static quenching), the reaction of the excited state, and transformation of energy, to name but a few.

In present study, the fluorescence quenching of α-glucosidase induced by imidazoquinazolines **19e** and **27e** was measured using a Synergy HTX multi-mode reader (Biotek Instruments, Winooski, VT, USA) equipped with a quartz cuvette of 10 mm. The excitation wavelength was set at 280 nm, and the emission spectra were reported at five different temperatures in the range from 300 to 450 nm with 10 accumulations for each collection point. The emission spectrum was corrected for the background fluorescence from the buffer solution and for the inner filter effect promoted by the inhibitors (Fig. 6). The active site of α-glucosidase contains tryptophan, tyrosine, and phenylalanine residues. As depicted in Fig. 6, fluorescence intensity of α-glucosidase increased to 340 nm,

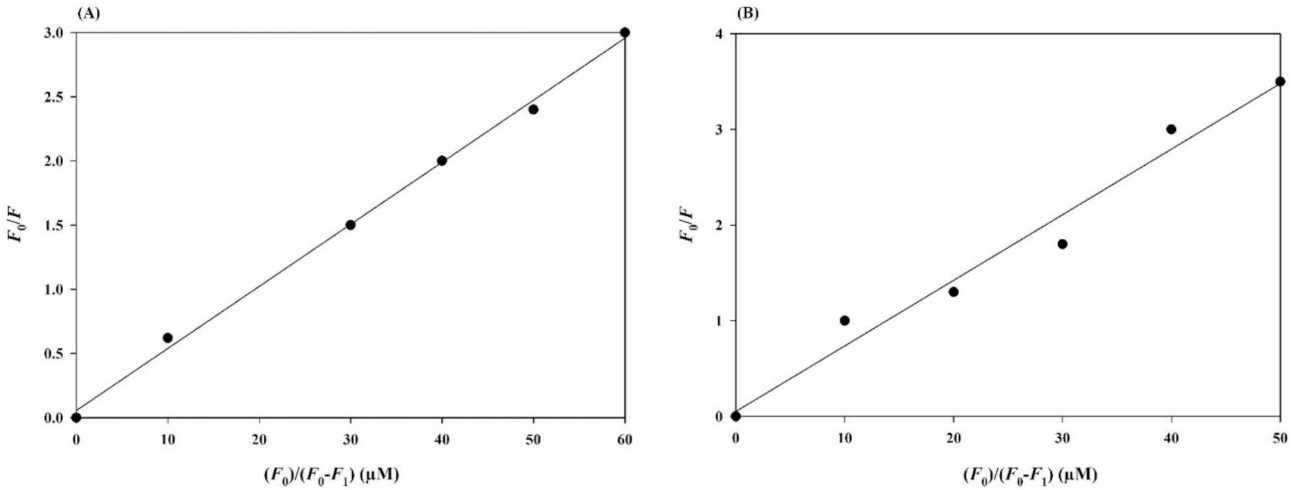

Fig. 7. The plots F_0/F Vs. function of $[D_t]$ $F_0/(F_0–F)$ at 20 °C: (**A**) imidazo[1,2-*c*]quinazoline **19e**; (**B**) benzo[4,5]imidazo[1,2-*c*]quinazoline **27e**.

Compound	K_A (L mol^{-1} s^{-1}) [a]	K_A (L mol^{-1} s^{-1}) [b]	n [b]	r [b]
19e	2.7×10^4	4.8×10^4	27	0.997
27e	5.0×10^4	6.8×10^4	16	0.999

Table 4. Binding constants and binding sites for imidazoquinazolines **19e** and **27e**. [a]Temperature is 60 °C. [b]Temperature is 20 °C.

followed by a subsequent decrease. Considering that the maximum intensity of tryptophan fluorescence occurs around 340 nm, it suggests that both imidazoquinazolines **19e** and **27e** created pivotal interactions tryptophan in the binding site of *α*-glucosidase, changing the enzyme's tertiary structure.

In addition to predicting the enzyme's tertiary structures in the presence of inhibitor, fluorescence spectroscopy assessments can provide insightful information about the binding constant, number of binding sites, and thermodynamic parameters of the studied interactions. Based on the results, imidazoquinazolines **19e** and **27e** proceeded static fluorescence quenching. Accordingly, the biding parameters were determined through the following equations:

The reaction is outlined as $P + D \rightarrow D_nP$; where P, D, and D_nP represent the protein, drug (inhibitor), and resulting complex molecule, respectively. Using Equation 1, the binding constant of this complex, denoted as K_A, is calculated.

$$K_A = \frac{n\,[D_nP]}{[D]\,n\,[P]} \tag{1}$$

The number of binding sites is denoted as "n" remaining unchanged in the static quenching mechanism. The number of the binding site of protein and drug is n and 1, respectively. Therefore, the equivalent concentration of the complex D_nP is $n[D_nP]$. The equivalent concentration of the protein is n[P], and the equivalent concentration of the drug is [D].

The total concentration of protein is $[P_t]$, and $[P_t]$ is $[P_f] + [D_nP]$. The total concentration of the drug is $[D_t]$, and $[D_f]$ is $[D_t]–n[D_nP]$. Since protein (P) is the only fluorescence in present study; therefore,

$$\frac{F_0}{F} = \frac{[P_t]}{[P_f]} \tag{2}$$

The fluorescence intensity of protein in the presence and absence of drug is F and F_0. The correlation between these intensities and $[D_t]$ is calculated in equation 3, by which the plot of F_0/F Vs. $[D_t]$ $F_0/(F_0–F)$ is outlined at 20 °C for both imidazoquinazolines **19e** and **27e** (Fig. 7). Moreover, using this equation, important parameters, including n and r at 20 °C, as well as K_A at 20 °C and 60 °C, are calculated, as listed in Table 4:

$$\frac{F_0}{F} = \frac{K_A\,[D_t]\,F_0}{(F_0 - F) - n\,K_A\,[P_t]} \tag{3}$$

The data in this Table 4 is graphed against temperature and binding constants, and important thermodynamic profile, including ΔG (free energy change), ΔH (enthalpy change), and ΔS (entropy change), could be computed through the equations as follow:

$$\ln \frac{K_{A2}}{K_{A1}} = \frac{\Delta H}{R}\left(\frac{1}{T_2} - \frac{1}{T_1}\right) \tag{4}$$

$$\Delta G = -RT \ln K_A = \Delta H - T\,\Delta S \tag{5}$$

The obtained results are presented in Table 5:

These figures are of great significance to determine the type of non-covalent forces between drug and enzyme's binding site, which are categorized into four groups: hydrophobic interaction, hydrogen bond, van der Waals forces, and electrostatic attraction. To identify the type of this interaction, the ΔH and ΔS values play a determining role, as follows: (1) $\Delta H > 0$, $\Delta S > 0$ indicating hydrophobic interactions; (2) $\Delta H < 0$, $\Delta S < 0$ indicating hydrogen bond and van der Waals interactions; (3) $\Delta H < 0$, $\Delta S > 0$ indicating van der Waals forces; and (4) $\Delta H < 0$, $\Delta S > 0$ indicating electrostatic interactions. Considering the signs of ΔH and ΔS as presented in Table 5, electrostatic forces were primarily formed between imidazoquinazolines **19e** or **27e** and the active site of *α*-glucosidase.

Molecular docking studies

Comprehensive molecular docking studies were performed on compounds **15**, **18**, **19**, **24**, **26**, and **27** using AutoDock4 and AutoDockTools (version 1.5.6) to analyze the interactions between the compounds and the crystal structure of *α*-glucosidase enzyme from *Saccharomyces cerevisiae*(PDB ID: 3A4A)[57]. As previously described in the SAR study, imidazo[1,2-*c*]quinazolines **15**, **18**, and **19** exhibited more favorable inhibitory potencies in comparison with their analog in benzo[4,5]imidazo[1,2-*c*]quinazoline **24**, **26**, and **27**. Moreover, the presence of amide functionality and 1,2,3-triazole ring played a crucial role in the inhibitory activities. Therefore, these computational studies were conducted to rationalize these orders and find notable interactions.

To begin with the comparison between imidazo[1,2-*c*]quinazolines **19a-h** and benzo[4,5]imidazo[1,2-*c*]quinazoline **27a-h**, it was observed that most of the derivatives, particularly compounds **19**, formed at least one hydrogen bond between Glu277 and one of the nitrogen atoms belonged to imidazole moiety of imidazoquinazoline core. Moreover, the imidazo[1,2-*c*]quinazolines **19** exhibited several interactions, including pi-lone pair**,** pi-cation/pi-anion, and pi-pi stacked bonds with the terminal phenyl moiety linked to the amide functionality of the compounds. However, these interactions were absent in the corresponding analogues from second series **27**. As depicted in Fig. 8, compounds **19** were able to form several electrostatic and hydrophobic interactions through its phenyl rings linked to imidazo[1,2-*c*]quinazoline backbone, while the number of interactions in benzo[4,5]imidazo[1,2-*c*]quinazoline backbones **27** was reduced. The same trend was observed for other derivatives in both series.

Up to this point, the superiority of compounds **19** over other series was established in both *in vitro* and *in silico* studies. Among them, compound **19e** with an IC_{50} value of 50 µM was the most potent derivative. Its binding energy affinity was -9.25 kcal/mol, remarkably better than that of acarbose (-5.01 kcal/mol) (Fig. 9). The binding mode of this compound was favorable for the formation of hydrogen bond with Arg315 and Asp352, a pi-sulfur bond with Phe178, as well as pi-pi bond between Tyr316 and the triazole ring. Further studies were also conducted on other compounds in the **19** series to find the key role of type of substituents and their positioning.

The difference between compounds **19a** and **19e** could be associated with the ability of amide functionality to act as a hydrogen bond donor or acceptor. In compound **19a**, the carbonyl group formed a hydrogen bond with Arg315; therefore, it was a hydrogen bond acceptor. However, in compound **19e**, N-H moiety formed a hydrogen bond with Tyr158; therefore, it was a hydrogen bond donor, which might be resulted from the presence of methoxy at C-2 position. To investigate the role of positioning, the molecular docking studies were also performed for compounds **19c** and **19d**. In compound **19c**, it was found that an unfavorable acceptor-acceptor bond was formed between carbonyl group and Gln353. Also, there were no interactions with the amide moiety in compound **19d**. In a general trend among compounds **19**, it was observed that chlorine caused a detrimental effect on the inhibitory activity (compounds **19f-19h**). This may be related to the chlorine atom's ability to hinder the amide functionality from acting as a hydrogen bond donor (Fig. 10).

To investigate the substantial role of amide moiety, the molecular docking studies were carried out for compounds **19a**, **19c**, **19f**, **27a**, **27c**, and **27f** as well as their analogues (compounds **18a-c** and **26a-c** in Table 2, which lack amide functionality). The NH-bond and / or carbonyl group of the amide functionality formed important hydrogen bonds with different aminoacids, including Arg315 in **19a**, Asp352 in **19c** and **27a**, Arg315 in **19f**, Gln353 in **27c**, and His280 in **27f**. It was concluded that the absence of amide moiety in compounds **18a-c** and **26a-c** caused the lack of noticeable hydrogen bonds, which might be responsible for their lower inhibitory potency. Fig. 11 is exemplifying this noticeable comparison between compounds **18a** and **19a**.

Compounds	K_A (L mol^{-1} s^{-1}) [a]	K_A (L mol^{-1} s^{-1}) [b]	ΔG (kJ mol^{-1})	ΔH (kJ mol^{-1})	ΔS (kJ mol^{-1})
19e	2.7×10^4	4.8×10^4	− 26.2	− 11.9	48.8
27e	5.0×10^4	6.8×10^4	− 27.0	− 6.4	70.5

Table 5. Thermodynamic parameters of imidazoquinazolines **19e** and **27e**. [a]Temperature is 60 °C. [b]Temperature is 20 °C.

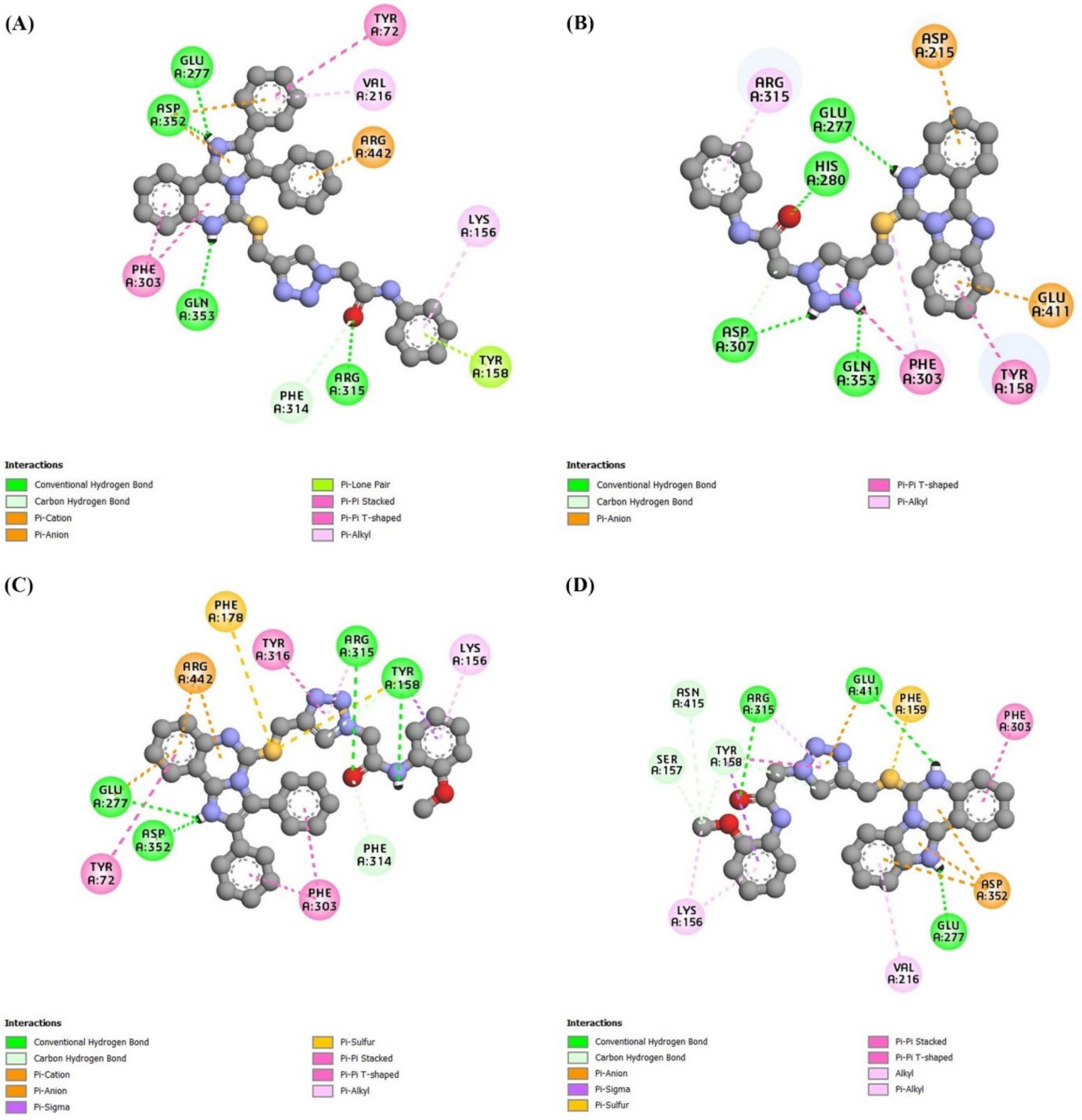

Fig. 8. 2D models of interactions in (**A**) **19a**; (**B**) **27a**; (**C**) **19e**; (**D**) **27e** with 3A4A.

To investigate the differences between **19a**, **19c**, **19f**, **27a**, **27c**, and **27f** as well as their analogues (compounds **15a-c** and **24a-c** in Table 2, which lack 1,2,3-triazole ring), it was found that the removal of triazole ring caused the loss of a crucial hydrogen bond with Glu277 (Fig. 12). This loss could be related with the different pose of the compound in the enzyme pocket, leading to a different distance between this amino acid and the imidazoquinazoline core. As shown in Fig. 13, the binding mode of compound **15a** was changed, resulting in an increased distance; consequently, the formation of the former hydrogen bond for compound **19a** was not possible anymore.

Conclusions

The study focused on the synthesis and evaluation of poly-substituted imidazo[1,2-*c*]quinazolines as potential *α*-glucosidase inhibitors. Among derivatives, compounds **19e** and **27e** were identified as the most effective inhibitors, significantly more potent than acarbose. Further analyses, including kinetic studies, circular dichroism, fluorescence spectroscopy, and thermodynamic profiling, revealed that these compounds inhibit *α*-glucosidase through competitive binding with the enzyme's active site, altering its secondary and tertiary

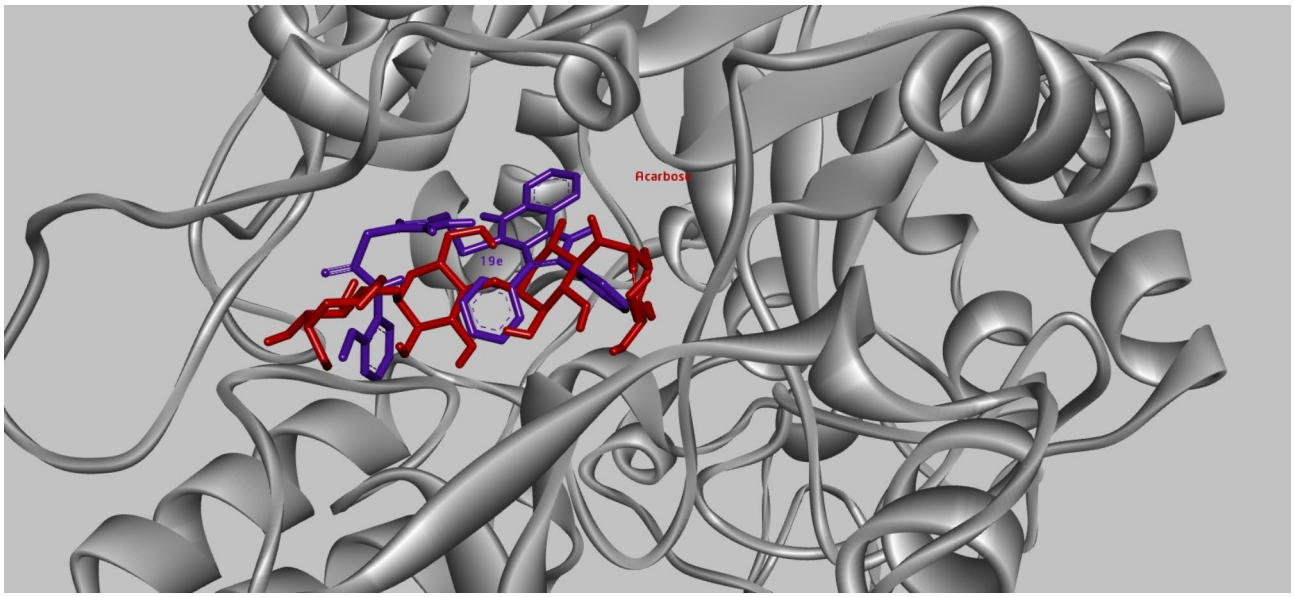

Fig. 9. Acarbose and compound **19e** are superimposed in the binding site of 3A4A.

structures. Moreover, thermodynamic parameters indicated spontaneous electrostatic interactions between the compounds and the enzyme. There was a great agreement between SAR analysis and molecular docking studies, confirming necessity of the presence of amide functionality and a 1,2,3-triazole ring for the inhibitory activity. These findings suggest that substituted imidazo[1,2-*c*]quinazolines are promising candidates for development of new *α*-glucosidase inhibitors.

Experimental

All chemicals were purchased from Merck (Germany) and were used without further purification. The reaction progress and the purity of synthesized compounds were monitored by thin-layer chromatography (TLC) on silica gel 250-micron F254 plastic sheets; zones were detected visually under UV light (254 nm). Melting points were measured on an Electrothermal 9100 apparatus. IR spectra were recorded on a Shimadzu IR-460 spectrometer. ^{1}H and ^{13}C NMR spectra were measured (DMSO-d_6 solution) with Bruker DRX-500 AVANCE (at 500.1 and 125.8 MHz) and Bruker DRX-400 AVANCE (at 400.1 and 100.1 MHz) instruments. Chemical shifts were reported in parts per million (ppm), downfield from tetramethylsilane. Proton coupling patterns were described as singlet (s), doublet (d), triplet (t), and multiplet (m). HRMS analysis was performed using a Waters Synapt G1 HDMS High Definition mass spectrometer equipped with an electrospray ionization (ESI) source. The samples were prepared by diluting the isolated compounds in methanol to a final concentration of 10 µg/mL. The analysis was conducted mainly in positive ion mode with a mass range of m/z 50–1000. Elemental analyses for C, H and N were performed using a Heraeus CHN-O-Rapid analyzer.

General synthetic procedures

2-Chloro-*N*-arylacetamides **3**, 2-azido-*N*-arylacetamides **5**, arylazides **7**, 2-(4,5-diphenyl-1*H*-imidazol-2-yl) aniline **12**, and 2-(1*H*-benzo[*d*]imidazol-2-yl)aniline **22**were synthesized using synthetic methods previously reported in the literature[54,58].

General procedure for the preparation of substituted imidazo[1,2-c]quinazoline-5-thiol (14 and 23)

A mixture of compound **12** or **22** (1 equiv.), CS_2 **13** (5 equiv.), KOH (2 equiv.) in EtOH was heated under reflux within 3h. After completion of the reaction as confirmed by TLC, the solvent was removed, and residue was poured into cool water. Subsequently, HCl was added gradually to the mixture to form precipitate. The resulting white powder was filtered and washed with great amount of water to yield in pure corresponding **14** and **23**.

General procedure for the preparation of substituted 2-(imidazo[1,2-c]quinazolin-5-ylthio)-N-arylacetamides (15 and 24)

To a stirring solution of compound **14** or **23** (1 equiv.) and K_2CO_3 (1.5 equiv.) in DMF at 80 °C, 2-Chloro-*N*-arylacetamides **3** (1.2 equiv.) was added gradually and heated for 12h. After completion of the reaction as confirmed by TLC, the reaction mixture was cooled to the ambient temperature. Subsequently, water was added to the mixture and extracted three times with EtOAc. The combined organic extracts were washed with brine, dried over Na_2SO_4 and then concentrated. Finally, the residue was recrystallized in EtOH to obtain the desired compounds **15** and **24**.

2-((2,3-diphenylimidazo[1,2-*c*]quinazolin-5-yl)thio)-*N*-phenylacetamide (15a):

Milky solid, mp 196–198 °C. IR (KBr) (ν_{max}/cm^{-1}): 3328 (NH), 1678 (C=O), 1597, 1473, 1339, 1278, 1198, 1106, 1082, 963, 855, 723, 635. ^{1}H NMR (400.1 MHz, DMSO-d_6): δ 10.50 (s, 1H, NH), 8.53 (d, J = 7.8 Hz, 1H,

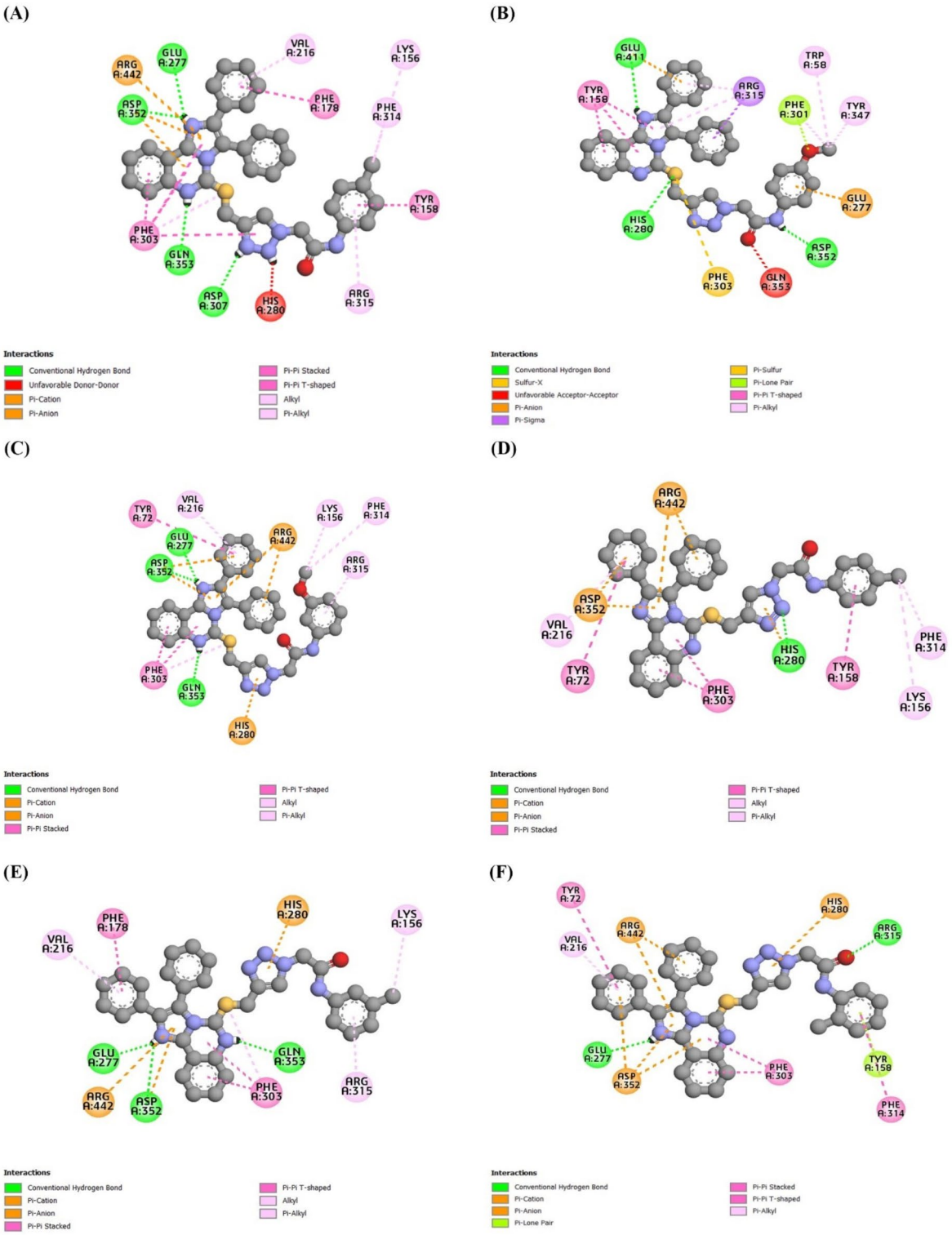

Fig. 10. 2D models of interactions in (**A**) **19b**; (**B**) **19c**; (**C**) **19d**; (**D**) **19e**; (**E**) **19g**; (**F**) **19h** with 3A4A.

CH), 7.95 (d, $J = 8.2$ Hz, 1H, CH), 7.79 (t, $J = 7.6$ Hz, 1H, CH), 7.72–7.45 (m, 11H, 11CH), 7.38–7.14 (m, 5H, 5CH), 4.73 (s, 2H, CH_2). HRMS (ESI) m/z for $C_{30}H_{23}N_4OS^+$ $[M + H]^+$, calculated: 487.1593, found: 487.1622. Anal. Calcd. for $C_{30}H_{22}N_4OS$: C, 74.05; H, 4.56; N, 11.51.; found: C, 74.32; H, 4.28; N, 11.67 %.

2-((2,3-diphenylimidazo[1,2-*c*]quinazolin-5-yl)thio)-*N*-(4-methoxyphenyl)acetamide (15b): Milky solid, mp 228–231 °C. IR (KBr) (ν_{max}/cm^{-1}): 3296 (NH), 1666 (C=O), 1562, 1499, 1453, 1398, 1342, 1293, 1297, 1083, 1011, 999, 865, 819, 767, 697, 637. ^{1}H NMR (400.1 MHz, DMSO-d_6): δ 10.11 (s, 1H, NH), 8.54 (d, $J = 7.8$ Hz, 1H, CH), 7.95 (d, $J = 8.0$ Hz, 1H, CH), 7.79 (t, $J = 7.5$ Hz, 1H, CH), 7.73–7.46 (m, 10H,

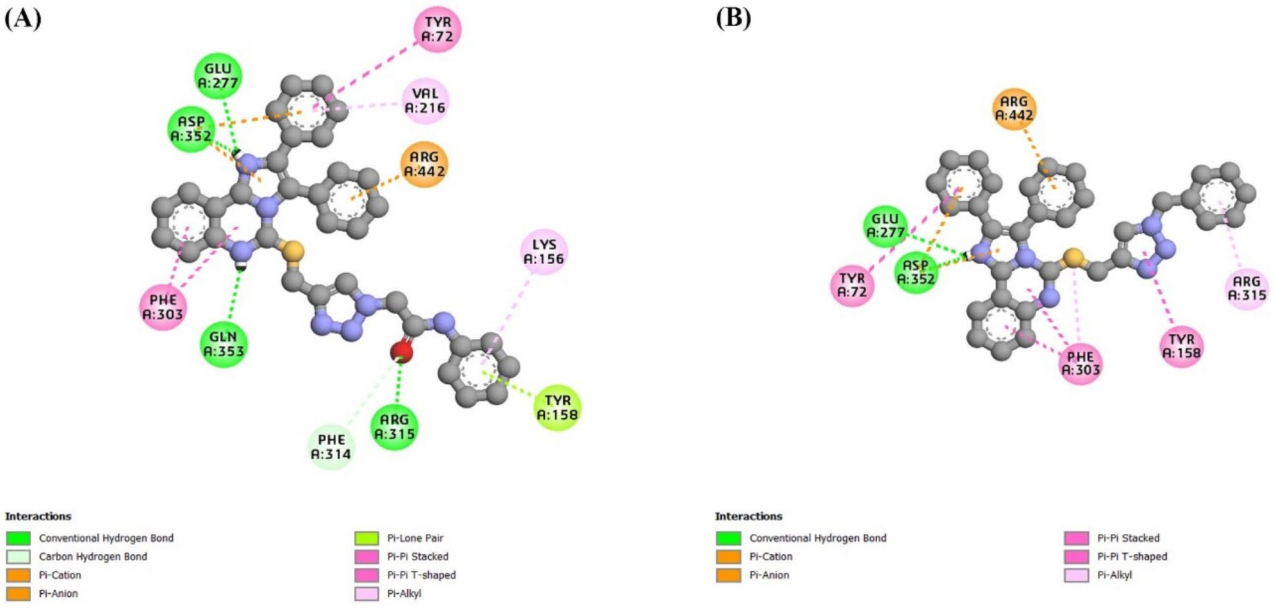

Fig. 11. 2D models of interactions in (**A**) **19a**; (**B**) **18a** with 3A4A.

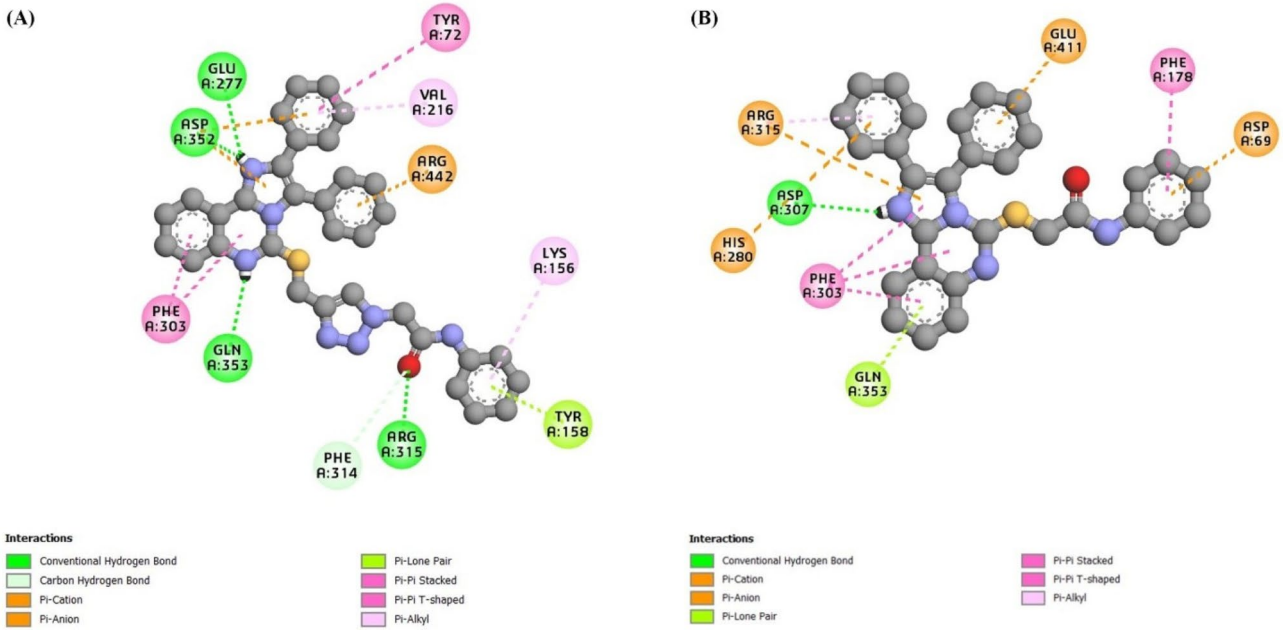

Fig. 12. 2D models of interactions in (**A**) **19a**; (**B**) **15a** with 3A4A.

10CH), 7.38–7.27 (m, 3H, 3CH), 6.95 (d, $J = 7.9$ Hz, 2H, 2CH), 4.78 (s, 2H, CH_2), 3.86 (s, 3H, OCH_3). HRMS (ESI) m/z for $C_{31}H_{25}N_4O_2S^+$ $[M + H]^+$, calculated: 517.1698, found: 517.1673. Anal. Calcd. for $C_{31}H_{24}N_4O_2S$: C, 72.07; H, 4.68; N, 10.85.; found: C, 72.34; H, 4.84; N, 11.08 %.

***N*-(4-chlorophenyl)-2-((2,3-diphenylimidazo[1,2-*c*]quinazolin-5-yl)thio)acetamide (15c):**

Milky solid, mp 242–245 °C. IR (KBr) (ν_{max}/cm^{-1}): 3278 (NH), 1686 (C=O), 1593, 1544, 1494, 1414, 1398, 1337, 1287, 1193, 1126, 1064, 994, 944, 788, 737, 699, 639. ^1H NMR (400.1 MHz, DMSO-d_6): δ 10.30 (s, 1H, NH), 8.55 (d, $J = 7.4$ Hz, 1H, CH), 7.97 (d, $J = 7.6$ Hz, 1H, CH), 7.78 (t, $J = 7.4$ Hz, 1H, CH), 7.70–7.45 (m, 10H, 10CH), 7.42–7.30 (m, 5H, 5CH), 4.75 (s, 2H, CH_2). HRMS (ESI) m/z for $C_{30}H_{22}ClN_4OS^+$ $[M + H]^+$, calculated: 521.1203, found: 521.1188. Anal. Calcd. for $C_{30}H_{21}ClN_4OS$: C, 69.16; H, 4.06; N, 10.75.; found: C, 68.98; H, 4.33; N, 10.92 %.

2-(benzo[4,5]imidazo[1,2-*c*]quinazolin-6-ylthio)-*N*-phenylacetamide (24a):

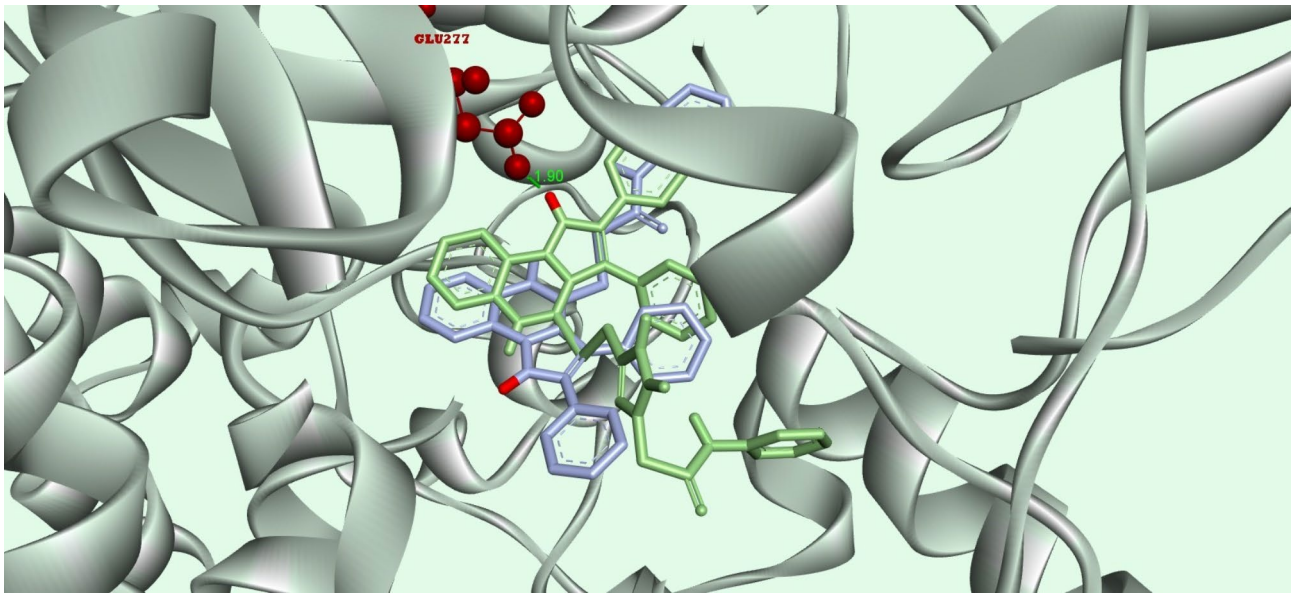

Fig. 13. 3D models of interactions of compound **19a** (green) vs. **15a** (blue) with 3A4A.

Yellow solid, mp 188–191 °C. IR (KBr) (ν_{max}/cm^{-1}): 3338 (NH), 1643 (C=O), 1523 1484, 1378, 1302, 1177, 1063, 966, 753, 685. ^{1}H NMR (500.1 MHz, DMSO-d_6): δ 10.94 (s, 1H, NH), 8.56 (d, J = 8.8 Hz, 1H, CH), 8.38 (d, J = 7.5 Hz, 1H, CH), 7.92–7.77 (m, 3H, 3CH), 7.61–7.52 (m, 3H, 3CH), 7.48–7.34 (m, 5H, 5CH), 4.80 (s, 2H, CH_2). HRMS (ESI) m/z for $C_{22}H_{17}N_4OS^+$ [M + H]$^+$, calculated: 385.1123, found: 385.1149. Anal. Calcd. for $C_{22}H_{16}N_4OS$: C, 68.73; H, 4.19; N, 14.57.; found: C, 68.56; H, 4.36; N, 14.79 %.

2-(benzo[4,5]imidazo[1,2-*c*]quinazolin-6-ylthio)-*N*-(4-methoxyphenyl)acetamide (24b):
Yellow solid, mp 206–208 °C. IR (KBr) (ν_{max}/cm^{-1}): 3298 (NH), 1677 (C=O), 1556, 1490, 1435, 1372, 1288, 1263, 1189, 1012, 988, 944, 899, 846, 793, 751, 622. ^{1}H NMR (500.1 MHz, DMSO-d_6): δ 10.63 (s, 1H, NH), 8.58 (d, J = 8.2 Hz, 1H, CH), 8.44 (d, J = 8.5 Hz, 1H, CH), 7.92 (d, J = 7.4 Hz, 1H, CH), 7.88 (d, J = 8.7 Hz, 1H, CH), 7.83 (t, J = 7.2 Hz, 1H, CH), 7.65–7.43 (m, 5H, 5CH), 7.00 (d, J = 8.7 Hz, 2H, 2CH), 4.75 (s, 2H, CH_2), 3.85 (s, 3H, OCH_3). HRMS (ESI) m/z for $C_{23}H_{19}N_4O_2S^+$ [M + H]$^+$, calculated: 415.1229, found: 415.1268. Anal. Calcd. for $C_{23}H_{18}N_4O_2S$: C, 66.65; H, 4.38; N, 13.52.; found: C, 66.83; H, 4.63; N, 13.36 %.

2-(benzo[4,5]imidazo[1,2-*c*]quinazolin-6-ylthio)-*N*-(4-chlorophenyl)acetamide (24c):
Yellow solid, mp 220–223 °C. IR (KBr) (ν_{max}/cm^{-1}): 3323 (NH), 1675 (C=O), 1608, 1584, 1522, 1477, 1453, 1388, 1257, 1227, 1166, 1076, 1029, 993, 875, 823, 783, 747, 623. ^{1}H NMR (500.1 MHz, DMSO-d_6): δ 10.98 (s, 1H, NH), 8.54 (d, J = 8.3 Hz, 1H, CH), 8.42 (d, J = 8.5 Hz, 1H, CH), 7.99–7.83 (m, 3H, 3CH), 7.67–7.51 (m, 5H, 5CH), 7.32 (d, J = 8.8 Hz, 2H, 2CH), 4.72 (s, 2H, CH_2). HRMS (ESI) m/z for $C_{22}H_{16}ClN_4OS^+$ [M + H]$^+$, calculated: 419.0733, found: 419.0698. Anal. Calcd. for $C_{22}H_{15}ClN_4OS$: C, 63.08; H, 3.61; N, 13.37.; found: C, 62.84; H, 3.83; N, 13.58 %.

General procedure for the preparation of substituted 5-(prop-2-yn-1-ylthio)imidazo[1,2-c]quinazoline (17 and 25)
A mixture of compound **14** or **23** (1 equiv.) and K_2CO_3 (1.5 equiv.) in DMF at ambient temperature was magnetically stirred for 30 min. Subsequently, propargyl bromide **16** (2 equiv.) was added, and then, the temperature was raised to 80 °C. After the reaction completed within an appropriate time, the reaction mixture was cooled to ambient temperature and introduced into the mixture of crushed ice and water. Over the next hour, the solid residue precipitated, which was then filtered and completely washed with water. Pure products **17** and **25** were obtained as a brown powder.

General procedure for the preparation of targeted compounds 18, 19, 26, and 27:
A mixture of compound **5** or **7** (1.2 equiv.), compound **17** or **25** (1 equiv.), $CuSO_4.5H_2O$ (0.3 equiv.), and sodium ascorbate (0.3 equiv.) in DMF was magnetically stirred at ambient temperature for an appropriate time until the starting materials were completely consumed. Then, water was introduced to the reaction mixture, and stirring continued until complete precipitation occurred. The resultant precipitate was filtered and thoroughly washed with enough amount of water. Finally, the solid was recrystallized in EtOH to afford pure, desired products in the form of milky powder.

5-(((1-benzyl-1*H*-1,2,3-triazol-4-yl)methyl)thio)-2,3-diphenylimidazo[1,2-*c*]quinazoline (18a):
Milky solid, mp 219–222 °C. IR (KBr) (ν_{max}/cm^{-1}): 1595, 1489, 1423, 1396, 1378, 1258, 1232, 1179, 1143, 1063, 996, 938, 848, 744, 650. ^{1}H NMR (500.1 MHz, DMSO-d_6): δ 8.50 (d, J = 7.7 Hz, 1H, CH), 8.13 (s, 1H, CH), 7.87 (d, J = 7.8 Hz, 1H, CH), 7.75 (t, J = 7.4 Hz, 1H, CH), 7.66 (t, J = 7.4 Hz, 1H, CH), 7.68–7.42 (m, 10H, 10CH), 7.35–7.14 (m, 5H, 5CH), 5.51 and 4.47 (2s, 4H, 2CH_2). HRMS (ESI) m/z for $C_{32}H_{25}N_6S^+$ [M + H]$^+$, calculated: 525.1861, found: 521.1879. Anal. Calcd. for $C_{32}H_{24}N_6S$: C, 73.26; H, 4.61; N, 16.02; found: C, 73.52; H, 4.78; N, 16.29 %.

5-(((1-(4-methoxybenzyl)-1*H*-1,2,3-triazol-4-yl)methyl)thio)-2,3-diphenylimidazo[1,2-*c*]quinazoline (18b):
Milky solid, mp 251–253 °C. IR (KBr) (ν_{max}/cm^{-1}): 1598, 1492, 1432, 1388, 1278, 1245, 1191, 1128, 1086, 1023, 1008, 996, 944, 898, 795, 753, 636. ^{1}H NMR (500.1 MHz, DMSO-d_6): δ 8.51 (d, J = 7.6 Hz, 1H, CH), 8.16 (s, 1H, CH), 7.82 (d, J = 8.0 Hz, 1H, CH), 7.75 (t, J = 8.2 Hz, 1H, CH), 7.66 (t, J = 7.4 Hz, 1H, CH), 7.71–7.50 (m, 6H, 6CH), 7.33–7.20 (m, 6H, 6CH), 6.91 (d, J = 8.7 Hz, 2H, 2CH), 5.67 and 4.47 (2s, 4H, 2CH$_2$), 3.63 (s, 3H, OCH$_3$). HRMS (ESI) m/z for $C_{33}H_{27}N_6OS^+$ [M + H]$^+$, calculated: 555.1967, found: 555.1939. Anal. Calcd. for $C_{33}H_{26}N_6OS$: C, 71.46; H, 4.72; N, 15.15; found: C, 71.68; H, 4.50; N, 15.38 %.
5-(((1-(4-chlorobenzyl)-1*H*-1,2,3-triazol-4-yl)methyl)thio)-2,3-diphenylimidazo[1,2-*c*]quinazoline (18c):
Milky solid, mp 268–272 °C. IR (KBr) (ν_{max}/cm^{-1}): 1538, 1487, 1436, 1364, 1348, 1329, 1291, 1278, 1230, 1173, 1074, 1044, 931, 855, 839, 769, 688. ^{1}H NMR (400.1 MHz, DMSO-d_6): δ 8.48 (d, J = 8.7 Hz, 1H, CH), 8.13 (s, 1H, CH), 7.85 (d, J = 8.4 Hz, 1H, CH), 7.74 (t, J = 7.2 Hz, 1H, CH), 7.65 (t, J = 7.2 Hz, 1H, CH), 7.62–7.57 (m, 3H, 3CH), 7.56–7.45 (m, 4H, 4CH), 7.34 (d, J = 8.4 Hz, 2H, 2CH), 7.30–7.19 (m, 5H, 5CH), 5.52 and 4.47 (2s, 4H, 2CH$_2$). HRMS (ESI) m/z for $C_{33}H_{24}ClN_6S^+$ [M + H]$^+$, calculated: 559.1472, found: 559.1438. Anal. Calcd. for $C_{33}H_{23}ClN_6S$: C, 68.62; H, 4.32; N, 15.00; found: C, 68.79; H, 4.58; N, 15.24 %.
2-(4-(((2,3-diphenylimidazo[1,2-*c*]quinazolin-5-yl)thio)methyl)-1*H*-1,2,3-triazol-1-yl)-*N*-phenylacetamide (19a):
Milky solid, mp 289–292 °C. IR (KBr) (ν_{max}/cm^{-1}): 3329 (NH), 1656 (C=O), 1528, 1484, 1377, 1327, 1289, 1233, 1188, 1069, 1022, 998, 845, 763, 695, 627. ^{1}H NMR (400.1 MHz, DMSO-d_6) δ 10.44 (s, 1H, NH-amid), 8.50 (d, J = 7.8 Hz, 1H, CH), 8.11 (s, 1H, CH), 7.92 (d, J = 8.1 Hz, 1H, CH), 7.74 (t, J = 7.5 Hz, 1H, CH), 7.69−7.45 (m, 10H, 10CH), 7.38−7.19 (m, 5H, 5CH), 7.07 (t, J = 7.3 Hz, 1H, CH), 5.27 and 4.55 (2s, 4H, 2CH$_2$). ^{13}C NMR (100.1 MHz, DMSO-d_6) δ 164.59, 147.90, 142.56, 140.98, 140.56, 138.84, 133.77, 133.74, 130.88, 129.85, 129.35, 128.69, 128.08, 127.71, 127.03, 126.16, 124.20, 123.08, 122.83, 119.62, 117.60, 52.65, 26.89. HRMS (ESI) m/z for $C_{33}H_{26}N_7OS^+$ [M + H]$^+$, calculated: 568.1920, found: 568.1889. Anal. Calcd. for $C_{33}H_{25}N_7OS$: C, 69.82; H, 4.44; N, 17.27; found: C, 70.03; H, 4.68; N, 17.43 %.
2-(4-(((2,3-diphenylimidazo[1,2-*c*]quinazolin-5-yl)thio)methyl)-1*H*-1,2,3-triazol-1-yl)-*N*-(*p*-tolyl) acetamide (19b):
Milky solid, mp 299–301 °C. IR (KBr) (ν_{max}/cm^{-1}): 3289 (NH), 1676 (C=O), 1577, 1533, 1485, 1453, 1378, 1329, 1267, 1174, 1075, 998, 893, 841, 762, 709, 688. ^{1}H NMR (400.1 MHz, DMSO-d_6) δ 10.35 (s, 1H, NH-amid), 8.50 (d, J = 7.8 Hz, 1H, CH), 8.11 (s, 1H, CH), 7.91 (d, J = 8.0 Hz, 1H, CH), 7.74 (t, J = 7.5 Hz, 1H, CH), 7.70−7.48 (m, 8H, 8CH), 7.43 (d, J = 8.2 Hz, 2H, 2CH), 7.32−7.18 (m, 3H, 3CH), 7.11 (d, J = 8.2 Hz, 2H, 2CH), 5.24 and 4.54 (2s, 4H, 2CH$_2$), 2.24 (s, 3H, CH$_3$). ^{13}C NMR (100.1 MHz, DMSO-d_6) δ 164.30, 147.90, 142.56, 140.98, 140.56, 136.32, 133.76, 133.74, 133.17, 130.87, 129.84, 129.71, 128.69, 128.08, 127.71, 127.04, 126.19, 123.08, 122.83, 119.62, 117.59, 52.64, 26.90, 20.90. HRMS (ESI) m/z for $C_{34}H_{28}N_7OS^+$ [M + H]$^+$, calculated: 582.2076, found: 582.2108. Anal. Calcd. for $C_{34}H_{27}N_7OS$: C, 70.20; H, 4.68; N, 16.86; found: C, 70.38; H, 4.84; N, 16.71 %.
2-(4-(((2,3-diphenylimidazo[1,2-*c*]quinazolin-5-yl)thio)methyl)-1*H*-1,2,3-triazol-1-yl)-*N*-(4-methoxyphenyl)acetamide (19c):
Milky solid, mp 342–345 °C. IR (KBr) (ν_{max}/cm^{-1}): 3348 (NH), 1668 (C=O), 1539, 1544, 1493, 1388, 1363, 1297, 1232, 1181, 1069, 1012, 978, 899, 833, 795, 744, 696, 682. ^{1}H NMR (400.1 MHz, DMSO-d_6) δ 10.30 (s, 1H, NH-amid), 8.50 (d, J = 7.8 Hz, 1H, CH), 8.10 (s, 1H, CH), 7.92 (d, J = 8.1 Hz, 1H, CH), 7.74 (t, J = 7.8 Hz, 1H, CH), 7.68−7.46 (m, 8H, 8CH), 7.46 (d, J = 8.1 Hz, 2H, 2CH), 7.34−7.16 (m, 3H, 3CH), 6.89 (d, J = 8.1 Hz, 2H, 2CH), 5.22 and 4.54 (2s, 4H, 2CH$_2$), 3.71 (s, 3H, OCH$_3$). ^{13}C NMR (100.1 MHz, DMSO-d_6) δ 164.04, 155.95, 147.92, 142.56, 140.98, 140.56, 133.77, 133.74, 131.92, 130.87, 129.86, 128.69, 128.08, 127.71, 127.03, 126.15, 123.08, 122.83, 121.17, 117.61, 114.43, 55.60, 52.57, 26.90. HRMS (ESI) m/z for $C_{34}H_{28}N_7O_2S^+$ [M + H]$^+$, calculated: 598.2025, found: 598.1994. Anal. Calcd. for $C_{34}H_{27}N_7O_2S$: C, 68.32; H, 4.55; N, 16.40; found: C, 68.58; H, 4.73; N, 16.56 %.
2-(4-(((2,3-diphenylimidazo[1,2-*c*]quinazolin-5-yl)thio)methyl)-1*H*-1,2,3-triazol-1-yl)-*N*-(3-methoxyphenyl)acetamide (19d):
Milky solid, mp 336–338 °C. IR (KBr) (ν_{max}/cm^{-1}): 3268 (NH), 1657 (C=O), 1535, 1505, 1474, 1422, 1358, 1299, 1232, 1183, 1096, 989, 923, 868, 835, 778, 726, 653. ^{1}H NMR (400.1 MHz, DMSO-d_6) δ 10.43 (s, 1H, NH-amid), 8.51 (d, J = 7.0 Hz, 1H, CH), 8.09 (s, 1H, CH), 7.93 (d, J = 7.2 Hz, 1H, CH), 7.76 (t, J = 7.1 Hz, 1H, CH), 7.70−7.47 (m, 8H, 8CH), 7.30−7.20 (m, 5H, 5CH), 6.66 (d, J = 7.3 Hz, 1H, CH), 5.25 and 4.55 (2s, 4H, 2CH$_2$), 3.71 (s, 3H, OCH$_3$). ^{13}C NMR (100.1 MHz, DMSO-d_6) δ 164.60, 159.98, 147.84, 142.56, 140.98, 140.55, 140.00, 133.75, 133.74, 130.86, 130.16, 129.81, 128.69, 128.09, 127.72, 127.04, 126.32, 123.08, 122.81, 117.56, 111.85, 109.66, 105.38, 55.42, 52.72, 26.88. HRMS (ESI) m/z for $C_{34}H_{28}N_7O_2S^+$ [M + H]$^+$, calculated: 598.2025, found: 598.2058. Anal. Calcd. for $C_{34}H_{27}N_7O_2S$: C, 68.32; H, 4.55; N, 16.40; found: C, 68.63; H, 4.69; N, 16.26 %.
2-(4-(((2,3-diphenylimidazo[1,2-*c*]quinazolin-5-yl)thio)methyl)-1*H*-1,2,3-triazol-1-yl)-*N*-(2-methoxyphenyl)acetamide (19e):
Milky solid, mp 318–321 °C. IR (KBr) (ν_{max}/cm^{-1}): 3269 (NH), 1678 (C=O), 1536, 1474, 1366, 1342, 1289, 1228, 1158, 1056, 1028, 918, 844, 795, 758, 656. ^{1}H NMR (400.1 MHz, DMSO-d_6) δ 9.70 (s, 1H, NH-amid), 8.49 (d, J = 7.7 Hz, 1H, CH), 8.10 (s, 1H, CH), 8.00−7.80 (m, 2H, 2CH), 7.73 (t, J = 7.3 Hz, 1H, CH), 7.70−7.42 (m, 8H, 8CH), 7.32−7.18 (m, 3H, 3CH), 7.09 (t, J = 7.6 Hz, 1H, CH), 7.05 (d, J = 7.0 Hz, 1H, CH), 6.89 (d, J = 7.8 Hz, 1H, CH), 5.36 and 4.54 (2s, 4H, 2CH$_2$), 3.84 (s, 3H, OCH$_3$). ^{13}C NMR (100.1 MHz, DMSO-d_6) δ 164.86, 149.97, 147.90, 142.55, 140.97, 140.56, 133.77, 133.74, 130.87, 129.85, 128.69, 128.08, 127.71, 127.02, 126.96, 126.19, 125.31, 123.08, 122.82, 122.13, 120.73, 117.59, 111.70, 56.14, 52.64, 26.90. HRMS (ESI) m/z for $C_{34}H_{28}N_7O_2S^+$ [M + H]$^+$, calculated: 598.2025, found: 598.1976. Anal. Calcd. for $C_{34}H_{27}N_7O_2S$: C, 68.32; H, 4.55; N, 16.40; found: C, 68.08; H, 4.74; N, 16.28 %.

***N*-(4-chlorophenyl)-2-(4-(((2,3-diphenylimidazo[1,2-*c*]quinazolin-5-yl)thio)methyl)-1*H*-1,2,3-triazol-1-yl)acetamide (19f):**
Milky solid, mp 358–361 °C. IR (KBr) (ν_{max}/cm^{-1}): 3302 (NH), 1662 (C=O), 1548, 1499, 1432, 1387, 1343, 1268, 1183, 1048, 1023, 988, 848, 772, 724, 688, 624. ^{1}H NMR (400.1 MHz, DMSO-d_6) δ 10.58 (s, 1H, NH-amid), 8.49 (d, J = 7.7 Hz, 1H, CH), 8.10 (s, 1H, CH), 7.91 (d, J = 8.0 Hz, 1H, CH), 7.74 (d, J = 7.6 Hz, 1H, CH), 7.70−7.46 (m, 10H, 10CH), 7.38 (d, J = 8.7 Hz, 2H, 2CH), 7.30−7.15 (m, 3H, 3CH), 5.27 and 4.54 (s, 4H, 2CH$_2$). ^{13}C NMR (100.1 MHz, DMSO-d_6) δ 164.81, 147.89, 142.55, 140.98, 140.56, 137.79, 133.76, 133.73, 130.87, 129.85, 129.28, 128.69, 128.08, 127.79, 127.71, 127.03, 126.15, 123.07, 122.83, 121.19, 117.60, 52.62, 26.88. HRMS (ESI) m/z for $C_{33}H_{25}ClN_7OS^+$ [M + H]$^+$, calculated: 602.1530, found: 602.1528. Anal. Calcd. for $C_{33}H_{24}ClN_7OS$: C, 65.83; H, 4.02; N, 16.28; found: C, 65.67; H, 4.28; N, 16.49 %.

***N*-(3-chlorophenyl)-2-(4-(((2,3-diphenylimidazo[1,2-*c*]quinazolin-5-yl)thio)methyl)-1*H*-1,2,3-triazol-1-yl)acetamide (19g):**
Milky solid, mp 339–342 °C. IR (KBr) (ν_{max}/cm^{-1}): 3278 (NH), 1674 (C=O), 1539, 1498, 1455, 1367, 1292, 1254, 1178, 1096, 1057, 1009, 932, 844, 787, 738, 727, 697, 623. ^{1}H NMR (400.1 MHz, DMSO-d_6) δ 10.64 (s, 1H, NH-amid), 8.49 (d, J = 7.3 Hz, 1H, CH), 8.13 (s, 1H, CH), 7.90 (d, J = 7.4 Hz, 1H, CH), 7.80−7.45 (m, 10H, 10CH), 7.40 (d, J = 7.3 Hz, 1H, CH), 7.35 (t, J = 7.6 Hz, 1H, CH), 7.30−7.18 (m, 3H, 3CH), 7.14 (d, J = 7.1 Hz, 1H, CH), 5.29 and 4.54 (2s, 4H, 2CH$_2$). ^{13}C NMR (100.1 MHz, DMSO-d_6) δ 165.03, 147.83, 142.56, 140.99, 140.55, 140.24, 133.74, 133.64, 131.08, 130.87, 130.83, 129.82, 128.69, 128.08, 127.72, 127.04, 126.28, 123.95, 123.07, 122.81, 119.14, 118.04, 117.57, 52.68, 26.88. HRMS (ESI) m/z for $C_{33}H_{25}ClN_7OS^+$ [M + H]$^+$, calculated: 602.1530, found: 602.1486. Anal. Calcd. for $C_{33}H_{24}ClN_7OS$: C, 65.83; H, 4.02; N, 16.28; found: C, 66.02; H, 4.24; N, 16.52 %.

***N*-(2-chlorophenyl)-2-(4-(((2,3-diphenylimidazo[1,2-*c*]quinazolin-5-yl)thio)methyl)-1*H*-1,2,3-triazol-1-yl)acetamide (19h):**
Milky solid, mp 329–332 °C. IR (KBr) (ν_{max}/cm^{-1}): 3324 (NH), 1658 (C=O), 1552, 1438, 1366, 1297, 1256, 1158, 1107, 1088, 999, 903, 845, 754, 729, 624. ^{1}H NMR (400.1 MHz, DMSO-d_6) δ 10.03 (s, 1H, NH-amid), 8.49 (d, J = 7.6 Hz, 1H, CH), 8.14 (s, 1H, CH), 7.89 (d, J = 7.9 Hz, 1H, CH), 7.78−7.40 (m, 11H, 11CH), 7.31 (d, J = 7.6 Hz, 1H, CH), 7.30−7.15 (m, 4H, 4CH), 5.39 and 4.54 (2s, 4H, 2CH$_2$). ^{13}C NMR (100.1 MHz, DMSO-d_6) δ 165.24, 147.82, 142.55, 140.98, 140.54, 134.55, 133.75, 133.73, 130.86, 130.82, 130.05, 129.81, 128.67, 128.08, 127.98, 127.72, 127.12, 127.00, 126.64, 126.23, 123.06, 122.81, 117.56, 52.46, 26.90. HRMS (ESI) m/z for $C_{33}H_{25}ClN_7OS^+$ [M + H]$^+$, calculated: 602.1530, found: 602.1563. Anal. Calcd. for $C_{33}H_{24}ClN_7OS$: C, 65.83; H, 4.02; N, 16.28; found: C, 66.04; H, 4.19; N, 16.11 %.

6-(((1-benzyl-1*H*-1,2,3-triazol-4-yl)methyl)thio)benzo[4,5]imidazo[1,2-*c*]quinazoline (26a):
Milky solid, mp 209–211 °C. IR (KBr) (ν_{max}/cm^{-1}): 1595, 1531, 1473, 1436, 1407, 1338, 1308, 1224, 1158, 1069, 974, 853, 807, 744, 668. ^{1}H NMR (400.1 MHz, DMSO-d_6) δ 8.54 (d, J = 8.4 Hz, 1H, CH), 8.35 (d, J = 7.3 Hz, 1H, CH), 8.31 (s, 1H, CH), 7.93 (d, J = 8.0 Hz, 1H, CH), 7.84 (d, J = 7.7 Hz, 1H, CH), 7.77 (t, J = 7.1 Hz, 1H, CH), 7.64−7.26 (m, 8H, 8CH), 5.71 and 4.75 (2s, 4H, 2CH$_2$). HRMS (ESI) m/z for $C_{24}H_{19}N_6S^+$ [M + H]$^+$, calculated: 423.1392, found: 423.1421. Anal. Calcd. for $C_{24}H_{18}N_6S$: C, 68.23; H, 4.29; N, 19.89; found: C, 68.45; H, 4.42; N, 19.76 %.

6-(((1-(4-methoxybenzyl)-1*H*-1,2,3-triazol-4-yl)methyl)thio)benzo[4,5]imidazo[1,2-*c*]quinazoline (26b):
Milky solid, mp 244–247 °C. IR (KBr) (ν_{max}/cm^{-1}): 1608, 1572, 1538, 1488, 1414, 1323, 1285, 1273, 1218, 1142, 1105, 954, 908, 866, 747, 668, 629. ^{1}H NMR (400.1 MHz, DMSO-d_6) δ 8.50 (d, J = 7.9 Hz, 1H, CH), 8.35 (d, J = 8.2 Hz, 1H, CH), 8.31 (s, 1H, CH), 7.94 (d, J = 8.1 Hz, 1H, CH), 7.85 (d, J = 8.0 Hz, 1H, CH), 7.80 (t, J = 7.1 Hz, 1H, CH), 7.70−7.44 (m, 5H, 5CH), 5.58 and 4.87 (2s, 4H, 2CH$_2$), 3.74 (s, 3H, OCH$_3$). HRMS (ESI) m/z for $C_{25}H_{21}N_6OS^+$ [M + H]$^+$, calculated: 453.1498, found: 453.1526. Anal. Calcd. for $C_{25}H_{20}N_6OS$: C, 66.35; H, 4.45; N, 18.57; found: C, 66.58; H, 4.63; N, 18.82 %.

6-(((1-(4-chlorobenzyl)-1*H*-1,2,3-triazol-4-yl)methyl)thio)benzo[4,5]imidazo[1,2-*c*]quinazoline (26c):
Milky solid, mp 252–254 °C. IR (KBr) (ν_{max}/cm^{-1}): 1591, 1501, 1475, 1336, 1296, 1224, 1158, 1104, 994, 905, 883, 828, 791, 627. ^{1}H NMR (400.1 MHz, DMSO-d_6) δ 8.50 (d, J = 7.9 Hz, 1H, CH), 8.38 (d, J = 8.3 Hz, 1H, CH), 8.31 (s, 1H, CH), 7.94 (d, J = 8.1 Hz, 1H, CH), 7.85 (d, J = 8.1 Hz, 1H, CH), 7.80 (t, J = 7.2 Hz, 1H, CH), 7.64 (t, J = 7.3 Hz, 1H, CH), 7.56 (t, J = 7.8 Hz, 1H, CH), 7.49 (t, J = 7.6 Hz, 1H, CH), 7.35 (d, J = 8.2 Hz, 2H, 2CH), 7.28 (d, J = 8.2 Hz, 2H, 2CH), 5.58 and 4.87 (2s, 4H, 2CH$_2$). HRMS (ESI) m/z for $C_{24}H_{18}ClN_6S^+$ [M + H]$^+$, calculated: 457.1002, found: 457.0968. Anal. Calcd. for $C_{24}H_{17}ClN_6S$: C, 63.08; H, 3.75; N, 18.39; found: C, 63.26; H, 3.99; N, 18.51 %.

2-(4-((benzo[4,5]imidazo[1,2-*c*]quinazolin-6-ylthio)methyl)-1*H*-1,2,3-triazol-1-yl)-*N*-phenylacetamide (27a):
Milky solid, mp 273–276 °C. IR (KBr) (ν_{max}/cm^{-1}): 3284 (NH), 1659 (C=O), 1573, 1463, 1459, 1367, 1308, 1298, 1155, 1083, 998, 923, 848, 755, 727, 691, 634. ^{1}H NMR (500.1 MHz, DMSO-d_6) δ 10.46 (s, 1H, NH-amid), 8.52 (d, J = 7.8 Hz, 1H, CH), 8.36 (s, 1H, CH), 8.32 (d, J = 7.6 Hz, 1H, CH), 7.93 (d, J = 7.8 Hz, 1H, CH), 7.85 (d, J = 7.6 Hz, 1H, CH), 7.77 (t, J = 7.4 Hz, 1H, CH), 7.70−7.30 (m, 7H, 7CH), 7.08 (t, J = 7.8 Hz, 1H, CH), 5.35 and 4.94 (2s, 4H, 2CH$_2$). ^{13}C NMR (125.1 MHz, DMSO-d_6) δ 164.52, 149.42, 147.15, 143.71, 142.11, 138.83, 132.55, 130.21, 129.35, 128.42, 127.59, 127.03, 126.82, 126.02, 124.23, 123.66, 120.00, 119.95, 119.66, 117.59, 115.25, 52.85, 26.40. HRMS (ESI) m/z for $C_{25}H_{20}N_7OS^+$ [M + H]$^+$, calculated: 466.1450, found: 466.1419. Anal. Calcd. for $C_{25}H_{19}N_7OS$: C, 64.50; H, 4.11; N, 21.06; found: C, 64.73; H, 4.28; N, 21.34 %.

2-(4-((benzo[4,5]imidazo[1,2-*c*]quinazolin-6-ylthio)methyl)-1*H*-1,2,3-triazol-1-yl)-*N*-(*p*-tolyl)acetamide (27b):
Milky solid, mp 284–286 °C. IR (KBr) (ν_{max}/cm^{-1}): 3228 (NH), 1656 (C=O), 1588, 1541, 1494, 1455, 1364, 1298, 1226, 1188, 1097, 1035, 941, 858, 802, 760, 724, 669, 635. ^{1}H NMR (500.1 MHz, DMSO-d_6) δ 10.35 (s, 1H, NH-amid), 8.52 (d, J = 7.6 Hz, 1H, CH), 8.40 (d, J = 7.8 Hz, 1H, CH), 8.30 (s, 1H, CH), 7.97−7.87 (m, 2H, 2CH), 7.80 (t, J = 7.4 Hz, 1H, CH), 7.64 (t, J = 7.5 Hz, 1H, CH), 7.56 (t, J = 7.4 Hz, 1H, CH), 7.50 (t, J =

7.2 Hz, 1H, CH), 7.43 (d, J = 7.6 Hz, 2H, 2CH), 7.10 (d, J = 7.6 Hz, 2H, 2CH), 5.30 and 4.93 (2s, 4H, $2CH_2$), 2.24 (s, 3H, CH_3). ^{13}C NMR (125.1 MHz, DMSO-d_6) δ 164.29, 149.47, 147.19, 143.88, 142.11, 136.32, 133.18, 132.51, 129.70, 128.93, 128.53, 127.58, 127.03, 126.43, 126.02, 124.24, 123.64, 120.04, 119.65, 117.06, 115.29, 52.74, 26.40, 20.90. HRMS (ESI) m/z for $C_{26}H_{22}N_7OS^+$ $[M + H]^+$, calculated: 480.1607, found: 480.1648. Anal. Calcd. for $C_{26}H_{21}N_7OS$: C, 65.12; H, 4.41; N, 20.45; found: C, 64.98; H, 4.62; N, 20.68 %.

2-(4-((benzo[4,5]imidazo[1,2-*c*]quinazolin-6-ylthio)methyl)-1*H*-1,2,3-triazol-1-yl)-*N*-(4-methoxyphenyl) acetamide (27c):

Milky solid, mp 299–302 °C. IR (KBr) (ν_{max}/cm^{-1}): 3266 (NH), 1678 (C=O), 1595, 1483, 1456, 1398, 1361, 1288, 1232, 1146, 1073, 1028, 999, 908, 761, 734, 695, 633. ^1H NMR (500.1 MHz, DMSO-d_6) δ 10.31 (s, 1H, NH-amid), 8.50 (d, J = 7.9 Hz, 1H, CH), 8.39 (d, J = 7.8 Hz, 1H, CH), 8.30 (s, 1H, CH), 7.95 (d, J = 7.0 Hz, 1H, CH), 7.88 (d, J = 7.6 Hz, 1H, CH), 7.79 (t, J = 7.8 Hz, 1H, CH), 7.70−7.40 (m, 5H, 5CH), 6.88 (d, J = 8.5 Hz, 2H, 2CH), 5.29 and 4.93 (2s, 4H, $2CH_2$), 3.71 (s, 3H, OCH_3). ^{13}C NMR (125.1 MHz, DMSO-d_6) δ 164.04, 155.99, 149.44, 147.14, 143.85, 142.11, 132.50, 131.93, 130.68, 128.89, 127.57, 127.01, 126.49, 126.00, 124.25, 123.63, 121.22, 120.03, 117.03, 115.27, 114.44, 55.61, 52.70, 26.38. HRMS (ESI) m/z for $C_{26}H_{22}N_7O_2S^+$ $[M + H]^+$, calculated: 496.1556, found: 496.1592. Anal. Calcd. for $C_{26}H_{21}N_7O_2S$: C, 63.02; H, 4.27; N, 19.79; found: C, 63.28; H, 4.09; N, 19.65 %.

2-(4-((benzo[4,5]imidazo[1,2-*c*]quinazolin-6-ylthio)methyl)-1*H*-1,2,3-triazol-1-yl)-*N*-(3-methoxyphenyl) acetamide (27d):

Milky solid, mp 272–275 °C. IR (KBr) (ν_{max}/cm^{-1}): 3281 (NH), 1663 (C=O), 1585, 1473, 1455, 1396, 1348, 1292, 1186, 1103, 1099, 1023, 975, 806, 774, 723, 689, 643. ^1H NMR (500.1 MHz, DMSO-d_6) δ 10.45 (s, 1H, NH-amid), 8.51 (d, J = 7.9 Hz, 1H, CH), 8.42−8.27 (m, 2H, 2CH), 7.93 (d, J = 7.7 Hz, 1H, CH), 7.86 (d, J = 7.2 Hz, 1H, CH), 7.78 (t, J = 7.8 Hz, 1H, CH), 7.61 (t, J = 7.6 Hz, 1H, CH), 7.54 (t, J = 7.7 Hz, 1H, CH), 7.46 (t, J = 7.4 Hz, 1H, CH), 7.27 (s, 1H, CH), 7.22 (t, J = 7.6 Hz, 1H, CH), 7.08 (d, J = 7.4 Hz, 1H, CH), 6.66 (d, J = 7.8 Hz, 1H, CH), 5.34 and 4.93 (2s, 4H, $2CH_2$), 3.71 (s, 3H, OCH_3). ^{13}C NMR (125.1 MHz, DMSO-d_6) δ 164.58, 160.00, 149.33, 147.11, 143.70, 142.08, 140.00, 132.50, 130.16, 128.78, 127.55, 127.01, 126.00, 125.26, 124.21, 123.63, 122.37, 119.97, 116.81, 115.22, 111.89, 109.71, 105.42, 55.43, 52.88, 26.38. HRMS (ESI) m/z for $C_{26}H_{22}N_7O_2S^+$ $[M + H]^+$, calculated: 496.1556, found: 496.1526. Anal. Calcd. for $C_{26}H_{21}N_7O_2S$: C, 63.02; H, 4.27; N, 19.79; found: C, 62.86; H, 4.39; N, 20.02 %.

2-(4-((benzo[4,5]imidazo[1,2-*c*]quinazolin-6-ylthio)methyl)-1*H*-1,2,3-triazol-1-yl)-*N*-(2-methoxyphenyl) acetamide (27e):

Milky solid, mp 258–261 °C. IR (KBr) (ν_{max}/cm^{-1}): 3314 (NH), 1675 (C=O), 1577, 1468, 1432, 1396, 1275, 1212, 1180, 1145, 1073, 1043, 1010, 913, 819, 761, 734, 695. ^1H NMR (500.1 MHz, DMSO-d_6) δ 9.69 (s, 1H, NH-amid), 8.53 (d, J = 8.1 Hz, 1H, CH), 8.40 (d, J = 7.7 Hz, 1H, CH), 8.31 (s, 1H, CH), 8.00−7.40 (m, 8H, 8CH), 7.22 (t, J = 7.6 Hz, 1H, CH), 7.07 (d, J = 7.4 Hz, 1H, CH), 6.89 (d, J = 7.6 Hz, 1H, CH), 5.42 and 4.93 (2s, 4H, $2CH_2$), 3.83 (s, 3H, OCH_3). ^{13}C NMR (125.1 MHz, DMSO-d_6) δ 164.77, 156.65, 149.98, 147.55, 143.70, 142.05, 140.00, 132.52, 130.81, 128.71, 127.56, 126.98, 126.01, 125.32, 124.19, 123.83, 123.65, 122.13, 120.73, 119.97, 117.95, 115.23, 111.73, 56.16, 52.84, 26.40. HRMS (ESI) m/z for $C_{26}H_{22}N_7O_2S^+$ $[M + H]^+$, calculated: 496.1556, found: 496.1586. Anal. Calcd. for $C_{26}H_{21}N_7O_2S$: C, 63.02; H, 4.27; N, 19.79; found: C, 63.22; H, 4.42; N, 19.99 %.

2-(4-((benzo[4,5]imidazo[1,2-*c*]quinazolin-6-ylthio)methyl)-1*H*-1,2,3-triazol-1-yl)-*N*-(4-chlorophenyl) acetamide (27f):

Milky solid, mp 309–312 °C. IR (KBr) (ν_{max}/cm^{-1}): 3268 (NH), 1654 (C=O), 1532, 1457, 1404, 1348, 1273, 1178, 1078, 1011, 962, 833, 786, 740, 655, 629. ^1H NMR (500.1 MHz, DMSO-d_6) δ 10.58 (s, 1H, NH-amid), 8.53 (d, J = 7.9 Hz, 1H, CH), 8.38 (d, J = 7.4 Hz, 1H, CH), 8.32 (s, 1H, CH), 7.94 (d, J = 7.8 Hz, 1H, CH), 7.88 (d, J = 7.6 Hz, 1H, CH), 7.79 (t, J = 7.7 Hz, 1H, CH), 7.70−7.50 (m, 5H, 5CH), 7.37 (d, J = 8.2 Hz, 2H, 2CH), 5.34 and 4.93 (2s, 4H, $2CH_2$). ^{13}C NMR (125.1 MHz, DMSO-d_6) δ 164.75, 149.39, 148.79, 143.75, 142.10, 137.80, 132.53, 130.70, 129.27, 128.86, 127.83, 127.60, 127.04, 126.61, 126.01, 124.25, 123.65, 121.22, 120.01, 116.98, 115.24, 52.78, 26.37. HRMS (ESI) m/z for $C_{25}H_{19}ClN_7OS^+$ $[M + H]^+$, calculated: 500.1060, found: 500.1091. Anal. Calcd. for $C_{25}H_{18}ClN_7OS$: C, 60.06; H, 3.63; N, 19.61; found: C, 60.18; H, 3.86; N, 19.48 %.

2-(4-((benzo[4,5]imidazo[1,2-*c*]quinazolin-6-ylthio)methyl)-1*H*-1,2,3-triazol-1-yl)-*N*-(3-chlorophenyl) acetamide (27g):

Milky solid, mp 292–294 °C. IR (KBr) (ν_{max}/cm^{-1}): 3268 (NH), 1654 (C=O), ^1H NMR (500.1 MHz, DMSO-d_6) δ 10.87 (s, 1H, NH-amid), 8.49 (d, J = 8.2 Hz, 1H, CH), 8.32 (d, J = 7.3 Hz, 1H, CH), 8.26 (s, 1H, CH), 7.96 (d, J = 8.4 Hz, 1H, CH), 7.90 (d, J = 7.2 Hz, 1H, CH), 7.85−7.28 (m, 8H, 8CH), 5.40 and 4.91 (2s, 4H, $2CH_2$). ^{13}C NMR (125.1 MHz, DMSO-d_6) δ 164.73, 149.86, 147.24, 143.80, 142.43, 134.89, 132.67, 130.78, 128.74, 128.12, 127.94, 127.65, 127.53, 127.36, 126.96, 126.57, 126.28, 125.81, 124.58, 123.00, 119.72, 117.41, 115.22, 52.10, 26.42. HRMS (ESI) m/z for $C_{25}H_{19}ClN_7OS^+$ $[M + H]^+$, calculated: 500.1060, found: 500.1076. Anal. Calcd. for $C_{25}H_{18}ClN_7OS$: C, 60.06; H, 3.63; N, 19.61; found: C, 60.24; H, 3.87; N, 19.47 %.

2-(4-((benzo[4,5]imidazo[1,2-*c*]quinazolin-6-ylthio)methyl)-1*H*-1,2,3-triazol-1-yl)-*N*-(2-chlorophenyl) acetamide (27h):

Milky solid, mp 279–282 °C. IR (KBr) (ν_{max}/cm^{-1}): 3342 (NH), 1666 (C=O), 1588, 1492, 1414, 1368, 1238, 1177, 1099, 1010, 956, 821, 785, 736, 686, 625. ^1H NMR (500.1 MHz, DMSO-d_6) δ 10.03 (s, 1H, NH-amid), 8.52 (d, J = 8.2 Hz, 1H, CH), 8.40 (d, J = 7.9 Hz, 1H, CH), 8.32 (s, 1H, CH), 7.96 (d, J = 7.8 Hz, 1H, CH), 7.90 (d, J = 7.9 Hz, 1H, CH), 7.81 (t, J = 7.6 Hz, 1H, CH), 7.75−7.45 (m, 5H, 5CH), 7.31 (d, J = 7.4 Hz, 1H, CH), 7.21 (t, J = 7.8 Hz, 1H, CH), 5.44 and 4.94 (2s, 4H, $2CH_2$). ^{13}C NMR (125.1 MHz, DMSO-d_6) δ 165.27, 149.45, 147.21, 143.79, 142.10, 134.57, 132.53, 130.06, 128.91, 128.00, 127.59, 127.14, 127.04, 127.03, 126.65, 126.28, 126.25, 126.03, 124.24, 123.67, 120.01, 117.00, 115.27, 52.53, 26.38. HRMS (ESI) m/z for $C_{25}H_{19}ClN_7OS^+$ $[M + H]^+$, calculated: 500.1060, found: 500.1108. Anal. Calcd. for $C_{25}H_{18}ClN_7OS$: C, 60.06; H, 3.63; N, 19.61; found: C, 60.31; H, 3.44; N, 19.86 %.

α-Glucosidase inhibition assay

α-Glucosidase enzyme ((EC3.2.1.20, Saccharomyces cerevisiae, 20 U/mg) and substrate (p-nitrophenyl glucopyranoside) were purchased from Sigma-Aldrich. Enzyme was prepared in potassium phosphate buffer (pH 6.8, 50 mM), as well as substituted imidazo[1,2-*c*]quinazolines **15a-c**, **18a-c**, **19a-h**, **24a-c**, **26a-c**, and **27a-h** were dissolved in DMSO (10% final concentration). The various concentrations of these compounds (20 mL), enzyme solution (20 mL) and potassium phosphate buffer (135 mL) were added in the 96-well plate and incubated at 37 °C for 10 min. Afterwards, the substrate (25 mL, 4 mM) was added to the mentioned mixture and allowed to incubate at 37 °C for 20 min. Finally, the change in absorbance was measured at 405 nm by using spectrophotometer (Gen5, Power wave xs2, BioTek, America). The percentage of enzyme inhibition was calculated using equation 1and IC_{50} values were obtained from non-linear regression curve using the Logit method.

$$\%\text{Inhibition} = \left[\left(\text{Abs}_{\text{control}} - \text{Abs}_{\text{sample}}\right)/\text{Abs}_{\text{control}}\right] \times 100 \tag{6}$$

Kinetic studies

The kinetic analysis was performed for the most potent compounds (**19e** and **27e**) to reveal the inhibition mode against α-glucosidase. The 20 mL of enzyme solution (1U/mL) was incubated with different concentrations of compound **19e** (0, 12.5, 25, and 50 µM) and compound **27e** (0, 15, 30, and 60 µM) for 15 min at 30 °C. Afterwards, various concentrations of substrate (p-nitrophenyl glucopyranoside, 1 to 10 mM) was added to measure the change of absorbance for 20 min at 405 nm by using spectrophotometer (Gen5, Power wave xs2, BioTek, America).

In the presence of a competitive inhibitor, K_m increases while V_{max} does not change. Michaelis–Menten saturation curve for an enzyme reaction shows the relation between the substrate concentration and reaction rate as bellow:

$$\frac{\text{v}}{V_{\max}} = \frac{[S]}{K\text{m}_{app} + [S]} \tag{7}$$

According to Michaelis–Menten graph, Km_{app} is also defined as:

$$K\text{m}_{app} = \left(1 + \frac{[\text{I}]}{K_{\text{I}}}\right) \tag{8}$$

[I] is the concentration of inhibitor.

Lineweaver Burk plot that provides a useful graphical method for analysis of the Michaelis–Menten is represented as:

$$\frac{1}{V_m} = \frac{K_m}{V_{max}}\left(1 + \frac{[\text{I}]}{K_{\text{I}}}\right)\frac{1}{[S]} + \frac{1}{\text{V}_{\max}} \tag{9}$$

Therefore, the slope of Lineweaver Burk plot is equal to:

$$\text{Slope} = \frac{K_m}{V_{max}}\left(1 + \frac{[\text{I}]}{K_{\text{I}}}\right) \tag{10}$$

The Km_{app} value is calculated by equation 6:

$$K\text{m}_{app} = K_m\left(1 + \frac{[\text{I}]}{K_{\text{I}}}\right) \tag{11}$$

Therefore, from replot of Km_{app} Vs. [I], equation 7 can be used for the calculation of K_I[59,60]:

$$Km_{app} = K_m + \frac{K_m}{K_{\text{I}}}[\text{I}] \tag{12}$$

Fluorescence spectroscopy measurements

This assay was carried out for the most potent derivative **19e** and **27e** to measure the fluorescence intensity. To this aim, different solutions containing different concentrations (0 to 1.0 µM) of the inhibitor and α-glucosidase (3 mL, 0.1 U/mL) were held for 10 min to equilibrate before measurements. Moreover, the fluorescence of the buffer containing compound **19e** and **27e**in the absence of the enzyme were subtracted as the background fluorescence. Afterwards, at the excitation wavelength of 280 nm, the fluorescence emission spectra were measured from 300 to 450 nm using a Synergy HTX multi-mode reader (Biotek Instruments, Winooski, VT, USA) equipped with a 1.0 cm quartz cell holder[61].

Molecular docking studies

Molecular docking study using AutoDock4 and Auto Dock Tools (version 1.5.6) was performed on substituted imidazo[1,2-*c*]quinazolines **15**, **18**, **19**, **24**, **26**, and **27** to elucidate the patterns of their interactions in the active site of α-glucosidase enzyme from *Saccharomyces cerevisiae* (PDB ID: 3A4A). Receptor was prepared by

removing water molecules and computing Kollman charges with BIOVIA Discovery Studio visualizer and Auto Dock Tools. To investigate the optimal docking grid, redocking process was performed with Acarbose as ligand, and RMSD value of 1.57 was achieved. Afterwards, ligands **15**, **18**, **19**, **24**, **26**, and **27** were prepared by adding Gasteiger Charges using Auto Dock Tools, and the docking procedure was conducted with 100 genetic algorithm runs using AutoDock4 and AutoGrid4. The interactions were visualized by PLIP online service and PyMOL Molecular Graphics System, Version 2.5.2 Schrödinger, LLC.

Data availability

Data is provided within the manuscript or supplementary information files.

Received: 20 August 2024; Accepted: 5 November 2024
Published online: 11 November 2024

Reference

1. ElSayed, N. A. et al. Introduction and methodology: Standards of care in diabetes—2023. *Am. Diabetes Assoc.* **46**, S1–S4 (2023).
2. Hossain, U., Das, A. K., Ghosh, S. & Sil, P. C. An overview on the role of bioactive α-glucosidase inhibitors in ameliorating diabetic complications. *Food Chem. Toxicol.* **145**, 111738. https://doi.org/10.1016/j.fct.2020.111738 (2020).
3. MD. https://www.who.int/news-room/fact-sheets/detail/diabetes.
4. Ghani, U. Re-exploring promising α-glucosidase inhibitors for potential development into oral anti-diabetic drugs: Finding needle in the haystack. *Eur. J. Med. Chem.* **103**, 133–162. https://doi.org/10.1016/j.ejmech.2015.08.043 (2015).
5. Wehmeier, U. & Piepersberg, W. Biotechnology and molecular biology of the α-glucosidase inhibitor acarbose. *Appl. Microbiol. Biotechnol.* **63**(613–625), 1. https://doi.org/10.1007/s00253-003-1477-2 (2004).
6. Peytam, F. et al. Synthesis and biological evaluation of new dihydroindolizino [8, 7-b] indole derivatives as novel α-glucosidase inhibitors. *J. Mol. Struct.* **1224**, 129290. https://doi.org/10.1016/j.molstruc.2020.129290 (2021).
7. Peytam, F. et al. Design and synthesis of new imidazo [1, 2-b] pyrazole derivatives, in vitro α-glucosidase inhibition, kinetic and docking studies. *Mol. Divers.* **24**, 69–80. https://doi.org/10.1007/s11030-019-09925-8 (2020).
8. Adib, M. et al. Design and synthesis of new fused carbazole-imidazole derivatives as anti-diabetic agents: In vitro α-glucosidase inhibition, kinetic, and in silico studies. *Bioorg. Med. Chem. Lett.* **29**, 713–718. https://doi.org/10.1016/j.bmcl.2019.01.012 (2019).
9. Adib, M. et al. New 6-amino-pyrido [2, 3-d] pyrimidine-2, 4-diones as novel agents to treat type 2 diabetes: A simple and efficient synthesis, α-glucosidase inhibition, molecular modeling and kinetic study. *Eur. J. Med. Chem.* **155**, 353–363. https://doi.org/10.1016/j.ejmech.2018.05.046 (2018).
10. Adib, M. et al. Design, synthesis and in vitro α-glucosidase inhibition of novel coumarin-pyridines as potent antidiabetic agents. *New J. Chem.* **42**, 17268–17278. https://doi.org/10.1039/C8NJ02495B (2018).
11. Ghomi, M. K. et al. Evaluation of novel 2-(quinoline-2-ylthio) acetamide derivatives linked to diphenyl-imidazole as α-glucosidase inhibitors: Insights from in silico, in vitro, and in vivo studies on their anti-diabetic properties. *Eur. J. Med. Chem.* **269**, 116332. https://doi.org/10.1016/j.ejmech.2024.116332 (2024).
12. Hu, C. et al. Synthesis and biological evaluation of indole derivatives containing thiazolidine-2, 4-dione as α-glucosidase inhibitors with antidiabetic activity. *Eur. J. Med. Chem.* **264**, 115957. https://doi.org/10.1016/j.ejmech.2023.115957 (2024).
13. Xiao, D. et al. Identification of 1, 3, 4-oxadiazolyl-containing β-carboline derivatives as novel α-glucosidase inhibitors with antidiabetic activity. *Eur. J. Med. Chem.* **261**, 115795. https://doi.org/10.1016/j.ejmech.2023.115795 (2023).
14. Feng, Q. et al. Synthesis, biological evaluation and action mechanism of 7H-[1, 2, 4] triazolo [3, 4-b][1, 3, 4] thiadiazine-phenylhydrazone derivatives as α-glucosidase inhibitors. *Eur. J. Med. Chem.* **262**, 115920. https://doi.org/10.1016/j.ejmech.2023.115920 (2023).
15. Ayan, E. K., Soyer, Z. & Uysal, Ş. Synthesis and enzymological characterization of some 2-(substitutedphenylamino) quinazolin-4 (3H)-one derivatives as potent α-glucosidase inhibitors in vitro. *Lett. Drug Des. Discov.* **18**, 723–732. https://doi.org/10.2174/1570180818999201224121929 (2021).
16. Babatunde, O., et al. Dihydroquinazolin-4 (1 H)-one derivatives as novel and potential leads for diabetic management. *Mol. Divers.* 1–20. https://doi.org/10.1007/s11030-021-10196-5 (2021).
17. El-Sayed, N. N. et al. Synthesis and evaluation of anticancer, antiphospholipases, antiproteases, and antimetabolic syndrome activities of some 3 H-quinazolin-4-one derivatives. *J. Enzyme Inhib. Med. Chem.* **34**, 672–683. https://doi.org/10.1080/14756366.2019.1574780 (2019).
18. Garlapati, R. et al. Development of α-glucosidase inhibitors by room temperature C-C cross couplings of quinazolinones. *Org. Biomol. Chem.* **11**, 4778–4791 (2013).
19. Gurram, V. et al. Design, synthesis, and biological evaluation of quinazoline derivatives as α-glucosidase inhibitors. *Med. Chem. Res.* **24**, 2227–2237. https://doi.org/10.1007/s00044-014-1293-5 (2015).
20. Ibrahim, A., Sakr, H. M., Ayyad, R. R. & Khalifa, M. M. Design, synthesis, in-vivo anti-diabetic activity, in-vitro α-glucosidase inhibitory activity and molecular docking studies of some quinazolinone derivatives. *ChemistrySelect* **7**, e202104590. https://doi.org/10.1002/slct.202104590 (2022).
21. Javaid, K. et al. 2-Arylquinazolin-4 (3H)-ones: A new class of α-glucosidase inhibitors. *Bioorg. Med. Chem.* **23**, 7417–7421. https://doi.org/10.1016/j.bmc.2015.10.038 (2015).
22. Khalifa, M. M., Sakr, H. M., Ibrahim, A., Mansour, A. M. & Ayyad, R. R. Design and synthesis of new benzylidene-quinazolinone hybrids as potential anti-diabetic agents: In vitro α-glucosidase inhibition, and docking studies. *J. Mol. Struct.* **1250**, 131768. https://doi.org/10.1016/j.molstruc.2021.131768 (2022).
23. Moheb, M. et al. Synthesis and bioactivities evaluation of quinazolin-4 (3 H)-one derivatives as α-glucosidase inhibitors. *BMC Chem.* **16**, 97. https://doi.org/10.1186/s13065-022-00885-z (2022).
24. Santos-Ballardo, L. et al. Synthesis, biological evaluation and molecular docking of 3-substituted quinazoline-2, 4 (1 H, 3 H)-diones. *J. Chem. Sci.* **132**, 1–10. https://doi.org/10.1007/s12039-020-01813-1 (2020).
25. Satyanarayana, N. et al. Synthesis of 2-styryl-quinazoline and 3-styryl-quinoxaline based sulfonate esters via sp 3 C-H activation and their evaluation for α-glucosidase inhibition. *New J. Chem.* **46**, 5162–5170. https://doi.org/10.1039/D1NJ05644A (2022).
26. Sinan Tokalı, F. Novel benzoic acid derivatives bearing quinazolin-4 (3H)-one ring: Synthesis, characterization, and inhibition effects on α-glucosidase and α-amylase. *ChemistrySelect* **7**, e202204019. https://doi.org/10.1002/slct.202204019 (2022).
27. Tokalı, F. S. et al. Design, synthesis, molecular docking, and some metabolic enzyme inhibition properties of novel quinazolinone derivatives. *Archiv. der Pharmazie* **354**, 2000455. https://doi.org/10.1002/ardp.202000455 (2021).
28. Wali, H. et al. Synthesis, in vitro, and in silico studies of newly functionalized quinazolinone analogs for the identification of potent α-glucosidase inhibitors. *J. Iran. Chem. Soc.* **18**, 2017–2034. https://doi.org/10.1007/s13738-021-02159-2 (2021).
29. Wei, M. et al. Quinazolinone derivatives: Synthesis and comparison of inhibitory mechanisms on α-glucosidase. *Bioorg. Med. Chem.* **25**(1303–1308), 1. https://doi.org/10.1016/j.bmc.2016.09.042 (2017).
30. Zhang, Y. et al. Quinazoline-1-deoxynojirimycin hybrids as high active dual inhibitors of EGFR and α-glucosidase. *Bioorg. Med. Chem. Lett.* **27**(4309–4313), 1. https://doi.org/10.1016/j.bmcl.2017.08.035 (2017).

31. Aroua, L. M. et al. A facile approach synthesis of benzoylaryl benzimidazole as potential α-amylase and α-glucosidase inhibitor with antioxidant activity. *Bioorg. Chem.* **114**, 105073. https://doi.org/10.1016/j.bioorg.2021.105073 (2021).
32. Arshad, T. et al. 5-Bromo-2-aryl benzimidazole derivatives as non-cytotoxic potential dual inhibitors of α-glucosidase and urease enzymes. *Bioorg. Chem.* **72**, 21–31. https://doi.org/10.1016/j.bioorg.2017.03.007 (2017).
33. Arshad, T. et al. Syntheses, in vitro evaluation and molecular docking studies of 5-bromo-2-aryl benzimidazoles as α-glucosidase inhibitors. *Med. Chem. Res.* **25**, 2058–2069. https://doi.org/10.1007/s00044-016-1614-y (2016).
34. Li, Y. et al. Discovery of new 2-phenyl-1H-benzo [d] imidazole core-based potent α-glucosidase inhibitors: Synthesis, kinetic study, molecular docking, and in vivo anti-hyperglycemic evaluation. *Bioorg. Chem.* **117**, 105423. https://doi.org/10.1016/j.bioorg.2021.105423 (2021).
35. Mohammadi-Khanaposhtani, M. et al. Synthesis, in vitro and in silico enzymatic inhibition assays, and toxicity evaluations of new 4, 5-diphenylimidazole-N-phenylacetamide derivatives as potent α-glucosidase inhibitors. *Med. Chem. Res.* **30**, 1273–1283. https://doi.org/10.1007/s00044-021-02734-5 (2021).
36. Özil, M., Parlak, C. & Baltaş, N. A simple and efficient synthesis of benzimidazoles containing piperazine or morpholine skeleton at C-6 position as glucosidase inhibitors with antioxidant activity. *Bioorg. Chem.* **76**, 468–477. https://doi.org/10.1016/j.bioorg.2017.12.019 (2018).
37. Rahim, F. et al. Synthesis, in vitro alpha-glucosidase inhibitory potential of benzimidazole bearing bis-Schiff bases and their molecular docking study. *Bioorg. Chem.* **94**, 103394. https://doi.org/10.1016/j.bioorg.2019.103394 (2020).
38. Taha, M. et al. Synthesis, α-glucosidase inhibitory, cytotoxicity and docking studies of 2-aryl-7-methylbenzimidazoles. *Bioorg. Chem.* **65**, 100–109. https://doi.org/10.1016/j.bioorg.2016.02.004 (2016).
39. Yar, M. et al. Organocatalyzed solvent free an efficient novel synthesis of 2, 4, 5-trisubstituted imidazoles for α-glucosidase inhibition to treat diabetes. *Bioorg. Chem.* **58**, 65–71. https://doi.org/10.1016/j.bioorg.2014.11.006 (2015).
40. Zawawi, N. K. N. A. et al. Synthesis, molecular docking studies of hybrid benzimidazole as α-glucosidase inhibitor. *Bioorg. Chem.* **70**(184–191), 1. https://doi.org/10.1016/j.bioorg.2016.12.009 (2017).
41. Viegas-Junior, C., Danuello, A., da Silva Bolzani, V., Barreiro, E. J. & Fraga, C. A. M. Molecular hybridization: A useful tool in the design of new drug prototypes. *Curr. Med. Chem.* **14**, 1829–1852. https://doi.org/10.2174/092986707781058805 (2007).
42. Carlucci, R., Lisa, M.-N. & Labadie, G. R. 1, 2, 3-Triazoles in biomolecular crystallography: A Geometrical Data-Mining Approach. *J. Med. Chem.* **66**, 14377–14390. https://doi.org/10.1021/acs.jmedchem.3c01097 (2023).
43. Yavari, A. et al. α-Glucosidase and α-amylase inhibition, molecular modeling and pharmacokinetic studies of new quinazolinone-1, 2, 3-triazole-acetamide derivatives. *Med. Chem. Res.* **30**, 702–711. https://doi.org/10.1007/s00044-020-02680-8 (2021).
44. Saeedi, M. et al. Design and synthesis of novel quinazolinone-1, 2, 3-triazole hybrids as new anti-diabetic agents: In vitro α-glucosidase inhibition, kinetic, and docking study. *Bioorg. Chem.* **83**, 161–169. https://doi.org/10.1016/j.bioorg.2018.10.023 (2019).
45. Wang, G., Peng, Z., Wang, J., Li, J. & Li, X. Synthesis and biological evaluation of novel 2, 4, 5-triarylimidazole–1, 2, 3-triazole derivatives via click chemistry as α-glucosidase inhibitors. *Bioorg. Med. Chem. Lett.* **26**, 5719–5723. https://doi.org/10.1016/j.bmcl.2016.10.057 (2016).
46. Saeedi, M. et al. Design, synthesis, in vitro, and in silico studies of novel diarylimidazole-1, 2, 3-triazole hybrids as potent α-glucosidase inhibitors. *Bioorg. Med. Chem.* **27**, 115148. https://doi.org/10.1016/j.bmc.2019.115148 (2019).
47. Deswal, L. et al. Synthesis and antidiabetic evaluation of benzimidazole-tethered 1, 2, 3-triazoles. *Archiv. der Pharmazie* **353**, 2000090. https://doi.org/10.1002/ardp.202000090 (2020).
48. Asemanipoor, N. et al. Synthesis and biological evaluation of new benzimidazole-1, 2, 3-triazole hybrids as potential α-glucosidase inhibitors. *Bioorg. Chem.* **95**, 103482. https://doi.org/10.1016/j.bioorg.2019.103482 (2020).
49. Peytam, F. et al. An efficient and targeted synthetic approach towards new highly substituted 6-amino-pyrazolo [1, 5-a] pyrimidines with α-glucosidase inhibitory activity. *Sci. Rep.* **10**, 2595. https://doi.org/10.1038/s41598-020-59079-z (2020).
50. Peytam, F. et al. Design, synthesis, molecular docking, and in vitro α-glucosidase inhibitory activities of novel 3-amino-2, 4-diarylbenzo [4, 5] imidazo [1, 2-a] pyrimidines against yeast and rat α-glucosidase. *Sci. Rep.* **11**, 11911. https://doi.org/10.1038/s41598-021-91473-z (2021).
51. Moghimi, S. et al. Design and synthesis of novel pyridazine N-aryl acetamides: In-vitro evaluation of α-glucosidase inhibition, docking, and kinetic studies. *Bioorg. Chem.* **102**, 104071. https://doi.org/10.1016/j.bioorg.2020.104071 (2020).
52. Firoozpour, L. et al. Synthesis, α-glucosidase inhibitory activity and docking studies of novel ethyl 1, 2, 3-triazol-4-ylmethylthio-5, 6-diphenylpyridazine-4-carboxylate derivatives. *BMC Chem.* **17**, 66. https://doi.org/10.1186/s13065-023-00973-8 (2023).
53. Firoozpour, L. et al. Design, synthesis and α-glucosidase inhibition study of novel pyridazin-based derivatives. *Med. Chem. Res.* **32**, 713–722. https://doi.org/10.1007/s00044-023-03027-9 (2023).
54. Peytam, F. et al. Imidazo [1, 2-c] quinazolines as a novel and potent scaffold of α-glucosidase inhibitors: design, synthesis, biological evaluations, and in silico studies. *Sci. Rep.* **13**, 15672. https://doi.org/10.1038/s41598-023-42549-5 (2023).
55. Nelson, D. L. L., A. L.; Cox, M. M. *Lehninger principles of biochemistry* (Macmillan, 2008).
56. Adler, A. *Methods in Enzymology* Vol. 27 (Academic Press, 1973).
57. Sakulkeo, O., Wattanapiromsakul, C., Pitakbut, T. & Dej-Adisai, S. Alpha-glucosidase inhibition and molecular docking of isolated compounds from traditional Thai medicinal plant, Neuropeltis racemosa Wall. *Molecules* **27**, 639. https://doi.org/10.3390/molecules27030639 (2022).
58. Tiew, K.-C. et al. Inhibition of Dengue virus and West Nile virus proteases by click chemistry-derived benz [d] isothiazol-3 (2H)-one derivatives. *Bioorg. Med. Chem.* **20**, 1213–1221. https://doi.org/10.1016/j.bmc.2011.12.047 (2012).
59. Dixon, M. The determination of enzyme inhibitor constants. *Biochem. J.* **55**, 170. https://doi.org/10.1042/bj0550170 (1953).
60. Todd, M. J. & Hausinger, R. Competitive inhibitors of Klebsiella aerogenes urease: Mechanisms of interaction with the nickel active site. *J. Biol. Chem.* **264**, 15835–15842. https://doi.org/10.1016/S0021-9258(18)71553-6 (1989).
61. Barker, M. K. & Rose, D. R. Specificity of processing α-glucosidase I is guided by the substrate conformation: Crystallographic and in silico studies. *J. Biol. Chem.* **288**, 13563–13574. https://doi.org/10.1074/jbc.M113.460436 (2013).

Acknowledgements

This work was supported and funded by grants No. 1400-2-104-54867 and 1403-1-104-71958 from the research council of Tehran University of Medical Sciences, Tehran, Iran.

Author contributions

A.F., L.F., and F.P. designed the study and conducted the experiments. F.P., F.S.H., R.F.M., and M.J.D.N. synthesized the targeted compounds. F.P., M.S.M., and B.B. wrote the manuscript, analyzed the characterization data, prepared the Supporting Information File, and carried out the docking studies. S.M. and M.A.F. performed the in vitro enzymatic analysis, kinetic study, circular dichroism spectroscopy, fluorescence spectroscopy measurements, and thermodynamic analysis. F.B., R.D., and M.B.T. revised the manuscript. M.N. and R.F. prepared the revised version of manuscript.

Declarations

Competing interests
The authors declare no competing interests.

Additional information
Supplementary Information The online version contains supplementary material available at https://doi.org/10.1038/s41598-024-78878-2.

Correspondence and requests for materials should be addressed to L.F. or A.F.

Reprints and permissions information is available at www.nature.com/reprints.

Publisher's note Springer Nature remains neutral with regard to jurisdictional claims in published maps and institutional affiliations.